UC Davis
UC Davis Previously Published Works

Title

Architecture and tectonostratigraphic evolution of the Pescadero Basin Complex, southern Gulf of California: Analysis of high-resolution bathymetry data and seismic reflection profiles

Permalink

https://escholarship.org/uc/item/0978j755

Authors

Ramírez-Zerpa, Néstor
Spelz, Ronald M
Yarbuh, Ismael
et al.

Publication Date

2022-03-01

DOI

10.1016/j.jsames.2021.103678

Peer reviewed

eScholarship.org Powered by the California Digital Library
University of California

Journal of South American Earth Sciences

Architecture and tectonostratigraphic evolution of the Pescadero Basin Complex, southern Gulf of California: Analysis of high-resolution bathymetry data and seismic reflection profiles

--Manuscript Draft--

Manuscript Number:	SAMES-D-21-00385R1
Article Type:	Research Paper
Keywords:	Pescadero Basin Complex, Gulf of California, Pull-apart basin geometry, Tectonostratigrpahic modeling
Corresponding Author:	Ronald M. Spelz, PhD Universidad Autónoma de Baja California - Campus Ensenada Ensenada, Baja California MEXICO
First Author:	Nestor Ramirez-Zerpa, Master
Order of Authors:	Nestor Ramirez-Zerpa, Master
	Ronald M. Spelz, PhD
	Ismael Yarbuh, PhD
	Raquel Negrete-Aranda, PhD
	Juan Contreras, PhD
	David A Clague, PhD
	Florian Neumann, PhD
	David W Caress, PhD
	Robert Zierenberg, PhD
	Antonio González-Fernández, PhD
Abstract:	The Pescadero Basin Complex (PBC) comprises three distinctive rhomb-shaped pull-apart basins separated by short and highly overlapped transform faults. Multibeam bathymetric data collected from ship at 40-m, combined with the interpretation of three 2D high-resolution multichannel seismic reflection profiles, were used to establish the architecture of the PBC. Detailed mapping and cross-sectional kinematic modeling based on the seismic images of the northern Pescadero basin reveal a highly evolved pull-part geometry, characterized by a well defined ~1.8 km-wide axial graben stretching ~32 km in a NNE-SSW direction. Among the fundamental elements controlling basin architecture and evolution of the PBC are the geometry of the initial configuration of the master strike-slip fault step-over and fault dynamics, which may cause transients in fault activity and basin reconfigurations. Structural analyses carried out in this study point out the PBC pull-apart basins developed under sustained transtensional deformation, where the relative motion of the crustal blocks is oblique and divergent to the transforms or principal displacement zones. We propose that the basin-crossing faults of the pull-apart basins comprising the PBC, initiated as synthetic Riedel faults and with progressive deformation, rotated clockwise around a vertical axis to acquire their present orientation. Basin-crossing faults with lesser obliquities control the subsidence along the basin-side faulted segments of the narrow graben systems that characterize the plate boundary at the corners of the PBC pull-apart basins. These narrow transtensional features may have served as connections facilitating marine waters to flood the PBC during the early stages of formation of the Gulf of California.
Suggested Reviewers:	Luis Mariano Cerca, Ph.D Associate Professor, Universidad Nacional Autonoma de Mexico mcerca@geociencias.unam.mx Line of research is relevant to this work
	Luca Ferrari, Ph.D Associate Professor, Universidad Nacional Autónoma de México: Universidad Nacional Autonoma de Mexico

Powered by Editorial Manager® and ProduXion Manager® from Aries Systems Corporation

	luca@unam.mx Dr. Ferrari has extensively work in the tectonic evolution of the Gulf of California
	Francisco Javier Nuñez-Cornú, Ph.D Associate Professor, Universidad de Guadalajara fcornu@pv.udg.mx Research line relevant to this work
	Joann M Stock, Ph.D Professor, Caltech: California Institute of Technology jstock@gps.caltech.edu Dr. Stock is an expert in the Gulf of California. Her 20+ years of experience working in the tectonic and magmatic evolution of the Gulf of California makes her the ideal reviewer for this work.
Opposed Reviewers:	
Response to Reviewers:	

Powered by Editorial Manager® and ProduXion Manager® from Aries Systems Corporation

REVISED Manuscript (text Unmarked)
Click here to access/download;REVISED Manuscript (text Unmarked);Revised Manuscript .docx
Click here to view linked References

Architecture and tectonostratigraphic evolution of the Pescadero Basin Complex, southern Gulf of California: analysis of high-resolution bathymetry data and seismic reflection profiles

Néstor Ramírez-Zerpa[1], Ronald M. Spelz[2]*, Ismael Yarbuh[2], Raquel Negrete-Aranda[3], Juan Contreras[4], David A. Clague[5], Florian Neumann[4], David W. Caress[5], Robert Zierenberg[6], Antonio González-Fernández[7]

[1]*Universidad Autónoma de Baja California. Posgrado en Oceanografía Costera, Facultad de Ciencias Marinas, Ensenada, B.C., México.*

[2]*Universidad Autónoma de Baja California. Departamento de Geología, Facultad de Ciencias Marinas, Ensenada, Baja California, México.*

[3]*Catedrático CONACyT, Laboratorio de Tectonofísica y flujo de calor, Departamento de Geología, Centro de Investigación Científica y de Educación Superior de Ensenada (CICESE). Ensenada, Baja California, México.*

[4]*Laboratorio de Tectonofísica y flujo de calor, Departamento de Geología, Centro de Investigación Científica y de Educación Superior de Ensenada (CICESE), Ensenada, Baja California, México.*

[5]*Monterrey Bay Aquarium Research Institute, Moss Landing, CA. USA.*

[6]*Earth and Planetary Sciences, University of California, Davis, CA, USA.*

[7] *Departamento de Geología, Centro de Investigación Científica y de Educación Superior de Ensenada (CICESE), Ensenada, Baja California, México.*

*corresponding author, rspelz@uabc.edu.mx

Abstract

The Pescadero Basin Complex (PBC) comprises three distinctive rhomb-shaped pull-apart basins separated by short and highly overlapped transform faults. Multibeam bathymetric data collected from ship at 40-m resolution, combined with the interpretation of three 2D high-resolution multichannel seismic reflection profiles, were used to establish the architecture of the PBC. Detailed mapping and cross-sectional kinematic modeling based on the seismic images of the North Pescadero Basin reveal a highly evolved pull-part geometry, characterized by a well defined ~1.8 km-wide axial graben extending ~32 km in a NNE-SSW direction. Among the fundamental elements controlling basin architecture and evolution of the PBC are the geometry of the initial configuration of the master strike-slip fault step-over and fault dynamics, which may cause transients in fault system activity and basin reconfigurations. Structural analyses carried out in this study point out the PBC pull-apart basins developed under sustained transtensional deformation, where the relative motion of the crustal blocks is oblique and divergent to the transforms or principal displacement zones. Cross-cutting relationships between the main fault systems controlling basin's subsidence and evolution, indicate that underdeveloped basin-crossing faults terminate against basin bounding normal faults, suggesting that ongoing pull-apart rifting continues to dominate basin evolution of the PBC. Furthermore, we propose that the undeveloped cross-basin faults of the PBC initiated as synthetic Riedel faults that, with progressive deformation along the divergent-wrench fault zone, rotated clockwise around a vertical axis to acquire their present orientation oblique to the master bounding transforms. Basin-crossing faults with lesser obliquities control the subsidence along the basin-side faulted segments of the narrow graben systems that characterize the plate boundary at the corners of the PBC pull-apart basins. These narrow transtensional synforms may have served as connections facilitating marine waters to flood the PBC during the early stages of formation of the Gulf of California.

Keywords: Pescadero Basin Complex; Gulf of California; pull-apart basin geometry; tectonostratigraphic modeling.

Highlights:

- Three-dimensional oblique rifting processes in the Gulf of California can be documented from high-resolution bathymetry data and 2D seismic reflection profiles.
- Tectonic geomorphology of the largely unexplored Pescadero Basin Complex is documented for the first time.
- Development and evolution of the Pescadero Basin Complex corroborate numerical and experimental models of pull-apart basin formation in oblique-divergent regimes.

1. Introduction

Transtensional and strike-slip faulting result from incremental changes in rift obliquity; a fundamental factor governing the geodynamic evolution of extensional systems (Brune et al., 2012; Brune et al., 2018). The Gulf of California (GoC) is an example of a young (~12.3 Ma) continental-rift margin characterized by an increasingly high-angle component of oblique-divergence resulting from the north-westward motion of the Pacific relative to the North American plate (Lonsdale, 1989; Stock and Hodges, 1989; Bohannon and Parsons, 1995; Atwater and Stock, 1998; DeMets, 1995; McQuarrie and Wernicke, 2005; Fletcher et al., 2007; Bennett et al., 2016; Umhoefer et al., 2020). Rift obliquity (i.e., angle between rift trend normal and plate displacement vector) along the GoC plate boundary has rapidly shifted from ~45 degrees ca. 10 Ma. to ~83 degrees in the present (Brune et al., 2018 and references therein). This rapid change is invoked by many authors as one of the leading factors enhancing the formation of pull-apart basins and associated energy-efficient strike-slip faults (e.g., Bennett & Oskin, 2014; Bennett, et al., 2016; Darin, et al., 2016; van Wijk, et al., 2017), boosting crustal thinning and eventual lithospheric rupture which resulted in the onset of seafloor spreading in the southern GoC (Umhoefer, 2011; Umhoefer, et al., 2018).

The southern GoC is an exemplary divergent margin to study the effects of a high-obliquity angle on strain localization, fault organization, basin architecture, and rift evolution (Figure 1; Atwater & Stock, 1998; Fletcher et al., 2007; Umhoefer, 2007; Umhoefer 2011; Bennett & Oskin, 2014; Bennett et al., 2016; Darin et al., 2016; van Wijk et al., 2017; Umhoefer et al., 2018; Umhoefer, et al., 2020). For example, the southern GoC reconciles several studies that suggest the increase in obliquity in divergent settings usually produces narrow rift valleys that progressively evolve into strike-slip dominated fault systems (e.g., Zwaan et al., 2016) and that high oblique angles (i.e., ~70 degrees) facilitate strain accommodation along strike-slip faults oriented parallel to the plate boundary (Withjack & Jamison, 1986; Richard & Cobbold, 1990; Tron & Brun, 1991; Fossen & Tikoff, 1993). In the latter model, the lateral component of transtensional shearing is assumed to be mechanically more efficient in concentrating the deformation in the upper crust, favoring subsequent lithospheric rupture through the formation of strike-slip faults and pull-apart basins (Brune et al., 2012; Darin et al., 2016; van Wijk et al., 2017; Brune et al., 2018).

Rupture of the continental lithosphere in the GoC occurred as early as 6 Ma in the Guaymas Basin, and ca. 3-3.5 Ma in the southernmost Alarcón Rise, whereas ca. 1-2 Ma in the basins located along the intervening gap between these two locations (Figure 1; DeMets, 1995; Lizarralde et al., 2007; Umhoefer, 2011 and references therein; Sutherland, et al., 2012). Thus, the southern GoC represents a unique domain where we can study the evolution of continental breakup and the onset of seafloor spreading throughout the last few million years. Moreover, the southern GoC is characterized by deep spreading centers with minimal sediment cover connected by relatively long transforms with considerable overlapping (e.g., van Wijk et al., 2017) that conform with classic plate tectonic models. This is one of very few young rifts where three-dimensional oblique rifting processes can be documented from surface geology (Diaz-Azpiroz et al., 2016).

The limited geophysical data coverage and the lack of seismic reflection transects across the southern GoC, however, have restricted the study of the crustal structure and the sediment infilling the basins. In particular, the Pescadero Basin Complex (PBC; Bischoff and Niemitz, 1980) consists of three pull-apart basins with rhomboidal geometry (South, Central and North Pescadero; Figure 2). Still, the kinematics of deformation and the role it plays in the formation of new oceanic crust remains poorly understood in this part of the rift system. In this study we provide new insights into the geometry, structural symmetry, internal structure and oblique rifting processes that led to the opening of the southern GoC. Based on high-resolution bathymetric data and 2D multichannel seismic data, we present a thorough description of the architecture of the PBC and discuss the fundamental elements controlling basin structure and evolution. Furthermore, our structural analysis shows that the PBC pull-apart basins developed under sustained transtensional deformation, where the relative motion of the crustal blocks is oblique and divergent to the transforms or principal displacement zones (PDZ's).

2. Regional Geology and Tectonics

2.1. Kinematic evolution of the Gulf of California

Even though the general history of the GoC is known, the details of its tectonic and kinematic evolution remain controversial despite thorough investigation by numerous authors (e.g., Stock & Hodges, 1989; Henry & Aranda-Gómez, 2000; Oskin & Stock, 2003; Aragón-Arreola & Martín-Barajas, 2007; Fletcher et al., 2007; Seiler et al., 2010; Brothers et al., 2012; Bennett et al., 2013; Ferrari et al., 2013; Bennett et al., 2016; Darin et al., 2016; Balestrieri et al., 2017; Persaud et al., 2017). Darin et al. (2016) present one the most comprehensive review to date, suggesting that the GoC broke up in three stages controlled by the motion of past and present tectonic plates. The first phase involved subduction of the Farallon plate beneath North America and calc-alkaline arc magmatism prior to 12.5 Ma. The second stage "proto-gulf" phase (~12.5-6 Ma) began with a major plate boundary reorganization following the cessation of subduction along most of the length of Baja California and the onset of volcanism related to partial melting by shear heating (Negrete-Aranda et al., 2013). Strain was focused on a sharp band forming a narrow rift and the first seafloor spreading centers began to develop in the southern region (Stock & Hodges, 1989; Lonsdale, 1989). The kinematics and strain distribution for that period are debatable (Darin et al., 2016), however between 8 to 6 Ma the motion of the Pacific plate relative to the North American plate rotated ~12º clockwise, from an azimuth of 300º to 312º, and the plate boundary started to accommodate oblique deformation (Spencer & Normark, 1979; Gans, 1997; Atwater & Stock, 1998; Fletcher et al., 2007; Darin et al., 2016)

The onset of oblique transtension at ~6 Ma marks the beginning of the third stage (Oskin et al., 2001; Darin et al., 2016, and references therein). Models and stratigraphic correlations indicate that during this last phase, up to 90% of the right lateral motion of the strike-slip faults along the western seaboard of Baja California, was transferred to the locus of the future gulf giving rise to the transtensional shear regime we observe today (Gastil et al., 1973; Abbott & Smith, 1989; Fletcher et al., 2007; Bennett et al., 2016; Darin et al., 2016; Balestrieri et al., 2017).

The swift opening of the GoC has been related to three main geodynamics factors (Umhoefer, 2011): 1) The presence of a weakened crust in a narrow area located between the Sierra Madre Occidental and the current Baja California Peninsula, 2) the moderately rapid relative plate motion (~51 km/Ma since ~12.5 Ma), and 3) the high obliquity angle that favored strike-slip faulting and the formation of transforming faults and pull-apart basins.

2.2. Seismotectonic framework of the southern Gulf of California

Tectonic activity in the southern GoC is characterized by an intricate array of faults and fracture zones cross-cutting the continental and oceanic crust (Figure 2). Seismicity records in this part of the rift system show that the vast majority of earthquakes with magnitude M>4 are located along the major transform faults such as the South Pescadero, Central Pescadero, Atl and Farallon, with fewer scattered events along the southeastern portion of the Baja California microplate and the sheared continental borderland west of the Baja peninsula (inset in Figure 2). Seismic activity is consistent with most of the Baja California microplate and North America shearing being accommodated by linked transform faults and short spreading centers along the gulf axis, at a rate of 45-47 mm/yr (Plattner et al., 2007), with an additional 4-6 mm/yr accommodated along the offshore Tosco-Abreojos fault zone southwest of the Baja California Peninsula (Umhoefer et al., 2020 and references therein).

3. High-resolution Bathymetry and Multi-channel Seismic data

3.1. High-resolution bathymetry data

Bathymetry data at 40-m resolution was collected during expedition FK181031 in November 2018 using the R/V *Falkor's* 30 kHz hull mounted Kongsberg EM302 multibeam sonar, focusing on the southern, central, and northern parts of the Pescadero Basin Complex (PBC), as well as the South Pescadero Transform, and the axis of the Alarcon Rise.

3.2. Multi-channel seismic data

Two-dimensional multi-channel reflection data across the PBC were collected in 2006 by CICESE's *R/V Francisco de Ulloa* in collaboration with Scripps Institution of Oceanography at UCSD. Seismic data acquisition was carried out using a two-bubble Sercel GI Air gun, with a total volume of 2458 cm^3 at 140 kg/cm^2 air pressure, as the seismic source. The GI Air gun consists of a generator that creates the acoustic pulse and an injector to reduce the collapse of the main bubble and its associated noise, enhancing its capabilities for the collection of high resolution marine seismic surveys. A towed hydrophone array of 48-channels (12.5 m group with 16 hydrophones per channel) recorded the airgun shots. The total streamer length was 600 m; the recording period was 6 s; the distance between sources was 37.5 m. Seismic reflection data were sampled at a rate of 1 ms, resulting in a total of 6000 samples per trace with a redundancy of 800%. The seismic reflection data were processed using the open source Seismic Unix software package (Stockwell, 1999). Processing was carried out in three stages: pre-stack, stack, and post-stack following the workflow described in Persaud et al. (2003) and references therein. The depths of reflectors were estimated using the conventional normal moveout procedure (NMO; see details in Sheriff and Geldart, 1995; Yilmaz, 2001).

Faults and shear zones were mapped and correlated across seismic lines to quantify the geometric and kinematic parameters of dip angle, sense of shear, and magnitude of horizontal and vertical displacement. These parameters are summarized for the seismic profile X-X' in supplemental Table S1. We also carried out a qualitative seismic attributes analysis of the seismic cross-sections. Elements such as lateral continuity, spatial variability, and internal geometry of the seismic reflectors were used to identify key structural, sedimentary, and volcanic features, as well as fluid-saturated strata, among others (e.g., Badley, 1985; Harding, 1990; Yilmaz, 2001; Lines & Newrick, 2004). Classification and interpretation of depositional facies in cross-section from the various seismic facies allowed us to identify variations in environmental conditions, which we interpret only in terms of changes in subsidence caused by tectonic events (Emery & Myers, 1996; Catuneanu, 2002).

4. Results

4.1. Two-Dimensional Architecture of the Pescadero Basin Complex

New bathymetric data allow us to interpret the tectonic geomorphology of the largely unexplored PBC for the first time. New insights into the three dimensional oblique-rifting processes affecting the southern GoC are revealed by geological details and structural descriptions of the entire complex derived from analysis of 40-m resolution bathymetry data.

The Pescadero Basin Complex (PBC)– The PBC's structural configuration and architecture is governed by the interaction of three right-lateral, right-stepping master fault systems with variable extents of separation and overlapping (Figures 2 and 3A). From south to north, these are the South Pescadero, Central Pescadero, and Atl transform faults. Relative motion across these sub-parallel fault systems and their associated secondary synthetic shear zones, have created a series of small strike-slip basins and large-scale pull-apart basins with distinct geometries. At least four distinctive pull-apart basin geometries are here identified. These range from the smallest 1) strike-slip basins, to the subtlest 2) connected depocenters with basin high, to the more prominent, mature, and highly evolved 3) stretched rhomboid and 4) spreading-segment basins (see Mann et al., 1983 and van Wijk et al., 2017 for a complete schematic overview of pull-apart basin geometries and evolution). Here we describe the geometry, structure, and main morphotectonic features of the largest and more evolved South, Central, and North Pescadero pull-apart basins in the PBC.

South Pescadero Basin (SPB) - The SPB is a sigmoidally shaped pull-apart basin with a pronounced Z-shape asymmetry developed between the South and Central Pescadero transform faults (Figure 3A). The length-to-width ratio of the basin, determined by the amount of fault overlap and separation between the master transforms is ~4:1, exceeding the global average of 3:1 observed for natural pull-apart basins (Aydin & Nur, 1982; Gürbüz, 2010 and references therein). The longitudinal margins of subsidence are controlled by a transverse system of oblique-extensional basin sidewall faults. The basin sidewall faults (BSFs) curve into an elongate sigmoidal shape in map view, linking with the bordering transforms that constitute the principal deformation zone (PDZ) on both sides of the basin (Figure 3A). The BSF system conveys displacement from one transform to the other above the stepover and is characterized by a left-stepping en-echelon geometry that branches out and above the opposing PDZ with an average strike 25^{o} clockwise to the trace of the PDZs.

The bridging path of the BSFs changes dramatically along strike as it becomes sub-perpendicularly oriented to the bounding PDZs towards the central portion of the basin. The BSFs with opposite dip polarity show intricate soft and hard-fault linkage patterns leading to the formation of a series of relay structures and ramps that shape the basin's NW and SE blocks. The resulting stair-like morphology is characteristic of a broad nested graben structure where rocks are successively displaced downward in the deepest part of the basin. The depocenter occurs in the northern half of the basin and is bounded longitudinally by oblique-normal fault segments. The younger, innermost basin faults are intimately associated with hydrothermal vent fields that discharge high temperature fluids into the hydrosphere (Paduan et al., 2018; Negrete-Aranda et al., 2021).

The northern and southern junctions of the stepover with the transforms are characterized by two narrow graben systems aligned with the trace of the transform’s PDZs (Figure 3A). Such features, characterized in cross-section by narrow V-shape grabens and negative flower structures, are common in divergent-wrench fault zones (e.g., Huang and Liu, 2017 and references therein), and have been identified as distinctive structural assemblies hosted in transtensional pull-apart basins (e.g., Wu et al., 2009). Both grabens are asymmetric and are bounded by oblique-normal faults with a sense of offset similar to the master South and Central Pescadero transforms, as suggested by structural criteria and geophysical data (Figures 3A and 3B). Both graben valleys, however, show distinct morphologies that we describe next.

The graben in the south corner is longer and wider than its counterpart in the north, and hosts an elongated depocenter located at the intersection of the splaying oblique-slip faults that bound the graben (Figure 3A). An intra-basin structural high, rising nearly 400 m above the deepest portion of the basin, separates two minibasins. This structural high is associated with local compressional stress resulting from the over-stepping geometry and kinematics of the right-lateral oblique-slip faults controlling the east and western margins of the graben valley, respectively (see converging black arrows in Figure 3A).

The northern graben occurs in the boundary between the South and Central Pescadero basins. It is shallower than its southern counterpart, lacks a distinctive depocenter, and shows a conical shape in map view that tapers towards the northwest. This morphology is consistent with a slight sinistral bend along a branch of the Central Pescadero Transform that controls the graben's eastern wall. The change of orientation along this segment of the master fault results in the formation of a contractional bend characterized by an elongated marginal ridge located along the footwall of the fault (Figure 3A). The ridge, oriented parallel to the NW-trending Central Pescadero's PDZ, is interpreted as a positive or hybrid flower structure (e.g., Huang and Liu, 2017) characterized by a shallow antiform and downward converging strands of reverse or oblique-normal faults, respectively, which merge at depth with a central subvertical strand of the Central Pescadero Transform.

Numerous submarine canyons, turbiditic channels, and slope gullies are common erosional features dissecting the uplifted NE margin of the SPB. Many of these channels, which represent the sediment routing system connecting the shallow continental platform with the deep interior of the basin, are oriented at high angles (~77º) to the bounding transforms and are presumably controlled by pre-existing brittle fabrics accommodating shear with a sense of offset opposite to the master transforms (Figure 3B).

Central Pescadero Basin (CPB) - CPB is located within the PDZ of the Central Pescadero Transform, which controls the southern end of the larger North Pescadero Basin. The CPB is a cone-shaped basin bounded to the west by the Central Pescadero Transform and to the east by a set of two right-stepping, oblique-slip faults: the Juno fault and the Kai fault, respectively. Both faults are synthetic to the Central Pescadero Transform and cut diagonally across the basin, with their traces terminating abruptly near the interior of the CPB and North Pescadero Basin, respectively (Figure 3A). Interaction between the Central Pescadero, Juno, and Kai faults results in a complex fault zone that divides the CPB into two discrete sub-basins with distinctive geometries and structural asymmetries. The smaller sub-basin, located in the southeastern corner is characterized by a long and narrow graben system in-line with the Central Pescadero transform (Figure 3A). The wedge-shape geometry of this graben valley is characterized by the intersection of the Central Pescadero Transform with the Juno fault, which controls the eastern margin of the graben. The depocenter is situated at this intersection, suggesting a northwestward decline in the vertical offset component accommodated by the main bounding faults (Figure 3A). The trace of oblique-slip faults that cut diagonally across the graben, occur along the entire length of the sub-basin but are more predominant and well developed in the northwestern end of the structure. There, an en-echelon array of left-stepping faults shows intricate soft and hard-linkage patterns, forming longer segments connecting with the main faults on opposite sides of the graben. The acute angle between the master bounding faults and their links ranges between 17^{o} and 27^{o}, averaging 23^{o}. This angle, however, increases northwestward as the array of left-stepping cross-basin faults dissects diagonally across a bathymetric structural high and connects with the bounding faults on opposite sides of the graben. The faulted bathymetric high, rising ~110 m above the basin floor of the CPB, represents the structural boundary between the two sub-basins (Figure 3A).

The northwestern sub-basin of the CPB is a rhomboid-shaped pull-apart bounded by the Central Pescadero and Kai faults. The length-to-width ratio of this sub-basin is 1:1, it has a Z-shape asymmetry, and its subsidence is controlled by a system of sigmoidally-shaped BSFs with oblique-slip kinematics and opposite dip polarity. The BSFs form a series of localized relay and breached ramps and join with the

NW-striking Central Pescadero and Kai faults to completely bound the sub-basin (Figure 3A). The sub-basin is asymmetric and, in contrast to the NW margin, the SE side is shallower and hosts wider ramps characterized by higher scarps controlled by a discrete array of west-dipping BSFs that connect the NW-striking Kai and Juno faults. The shallower depths characterizing the SE margin of the sub-basin are consistent with its location on the footwall of the Juno fault, which in turn controls the subsidence along the bordering wedge-shaped graben previously described. The Juno fault cuts diagonally across the CPB, and its termination near the central portion of the basin coincides with the sub-basin depocenter (Figure 3A). The oval-shaped depocenter is oriented sub parallel to the Juno fault, suggesting the fault exerts strong control on the subsidence of the basin. Farther north, the depth of the CPB gradually decreases across a series of closely spaced ramps developed along the array of east-dipping BSFs that control the NW margin of the basin. This margin lies along a subtle NE-oriented ridge that separates the CPB from the southern portion of the North Pescadero Basin. The ridge is bounded on both sides by BSFs with opposite polarities that successively displace rocks downward in the deeper portions of the neighboring basins. The central portion of the dividing ridge is associated with subvertical BSFs accommodating lateral shear with a sense of offset opposite to the master transforms, as suggested by the local fault plane solutions (Figure 3B).

North Pescadero Basin (NPB) - NPB is the largest and most evolved pull-apart basin in the PBC. Its flanks are characterized by several fan and turbiditic channels, slope gullies, and submarine canyons that are widely exposed over ~35-45 km-wide strips of continental shelf along the mainland and Baja California sheared margins (Figure 3A). The basin is formed at the overstep between the overlapping Central Pescadero and Atl transform faults, and has a spreading-segment architecture with a Z-shape geometry. The length-to-width ratio of the basin is ~2.5:1, only slightly below the global average ratio of 3:1 (Aydin & Nur, 1982). The basin is symmetric and its longitudinal margins of subsidence are controlled by a system of BSFs with normal and oblique-slip kinematics (Figures 3A and 3B). BSFs are oriented at high angles (>65-80º) to the bordering Central Pescadero and Atl transforms, and connect directly to the PDZs to completely bound the basin (Figure 3A). Discrete focal mechanisms associated with these faults indicate normal to oblique-slip kinematics with a sense of offset opposite to the master transforms (Figure 3B). At the intersection with the PDZs, the BSFs curve into a sigmoidal shape and form a staggered pattern with a left-stepping geometry. The acute angle between the BSFs and the PDZs varies between 21ºand 40º, averaging 31º. Differential hanging-wall displacements along the bounding BSFs with opposite dip-directions have resulted in a narrow nested graben that characterizes the basin's interior. The axial graben extends ~32 km in a NNE-SSW direction, and its innermost walls are controlled by an intricate array of sub-parallel BSFs that closely follow the -3280 m bathymetric contour (Figure 3A). A small depocenter exists in the southern third of the axial graben, where the structure becomes wider (~3.6 km), deeper (-3332 mbsl), and flatter along the boundary with the CPB at its SW end. The northern corner of the NPB is also characterized by a prominent graben valley in-line with the Atl transform. The graben shows minimal structural and geometric variations along-strike and hosts an elongated depocenter (-3380 mbsl) oriented at an angle of 23º clockwise to the trace of the bounding master faults. This acute angle is consistent with the orientation of a few discrete strands of BSFs that can be observed cutting diagonally across the valley floor. A group of small-scale pull-apart basins are also exposed in the NW portion of the NPB. These basins occur at the tips of synthetic fault segments associated with the Santa Cruz fault zone and the Atl transform, respectively (Figure 3A).

4.2. Cross-sectional structure and seismic stratigraphy of the Central and North Pescadero basins

In this section we perform a structural, stratigraphic and lithological interpretation of three multichannel seismic sections (profiles X-X', Y-Y' and Z-Z' in Figures 4, 5 and 6) across the northern segment of the PBC from which we build a model of episodes of deposition and tectonic subsidence for the entire basin.

The seismic section X-X' is oriented NE and transects the CPB between the Cerralvo extensional system on the west (Macias-Iñiguez et al., 2019) and the sheared continental margin of Sinaloa on the east (Figure 4). The CPB results from both strike-slip and dip-slip movement along the Central Pescadero

Transform, the Kai fault, and the northern Santa Cruz fault zone (Figures 3A and 4). These structures are recognized in the seismic profiles by their uplifted footwall blocks and active degradation. The cross-section also reveals that subsidence appears to be approximately twice the sedimentation rate. A significant fraction of this subsidence is being accommodated by a number of smaller faults dissecting the central depression, in which fault dip increases progressively towards the basin's depocenter (Figure 4). This pattern suggests these faults possibly intersect each other at deeper structural levels. An analysis of these structures and quantification of the strain accommodated by faulting show a stretch factor, s, of ~2.0 and a linear strain ε of 96% (see Figure S1 and Table S1) consistent with estimates by other authors across surrounding basins (e.g., Páramo et al. 2008; Brothers et al. 2012; Bot et al. 2016; and Macias-Iñiguez et al. 2019).

A series of sharp, high amplitude and frequency reflections separating subhorizontal or gently dipping strata reflections from underlying heterogeneous and poorly coherent reflections were also identified in the profiles. These reflections, which are interpolated and labeled as L-0 in Figures 4, 5 and 6, likely correspond to basement meta-volcanic and meta-sedimentary rocks (Aranda-Gómez and Pérez-Venzor, 1988; Schaaf et al., 2000; Fletcher et al., 2003; Montrella, 2004; Duque-Trujillo et al., 2015; Bot et al., 2016; Balestrieri et al., 2017; Macias-Iñiguez et al., 2019) of Jurassic-Tertiary age that predate the sedimentary successions deposited during the opening of the gulf. Within this package, a series of third-order sequences (0.5 to 5 Ma) and associated bounding surfaces can be identified, which reflect a series of environmental changes in sedimentation.

The most basal succession S-1 lies unconformably on the acoustic basement L-0 and has a chaotic structure with low coherence, diagnostic of poor stratification (Figure 4). This sequence marks the beginning of the rift opening as the bounding surface L-1 dies out towards the F-7 fault, whereas it tapers in the eastward direction. These seismic facies are interpreted as hummocky coarse-grain sediments derived from sources close to the basin. The L-2 sequence boundary defines a thin stratal succession S-2 with strong seismic coherence and continuity, suggesting a change in environmental conditions, which we interpret as the beginning of the first marine incursions into the PBC. The sequence S-2 onlaps the surface

L-1 towards the east margin, while it is being juxtaposed against the Central Pescadero Transform on the west. This is evidence of a westward migration of fault activity. During the deposition of S-2 the faults F-6 and F-5 ruptured on the surface but were quickly abandoned (see Figure 7). From this time onward, the Central Pescadero Transform acted as the master bounding fault.

In contrast, the eastern margin of the basin deformed by flexure leading to the deposition of convergent stratal geometries. This reorganization was accompanied by a rapid deepening in the depositional regime as inferred from sequences S-3 to S-7. The S-3 sequence consists of bundles of moderately coherent reflectors, typical of transitional or continental shelf environments. The upper sedimentary packages S-4, S-5, S-6 and S7, however, become more coherent and cyclical (Figure 4) and are interpreted as intercalations of fine sand, silt, and hemipelagic sediments (Chopra & Martfurt, 2007).

The seismic section Y-Y’ (Figure 5) has an orientation of NNW-SSE, nearly perpendicular to section X-X' and the extensional faults in the NPB and CPB. The interpretation of the Y-Y' line, shown in Figures 5B and 5C, was constructed by matching the seismic markers L-0 through L-7 against the uninterpreted section at the intersection of the X-X' and Y-Y' profiles. Then, we imported the markers into the uninterpreted section following the stratification. The seismic facies on both lines are highly correlated indicating that the environmental changes observed across the southern shear zone are basinwide despite changes in faulting style and intensity. In the Y-Y' seismic section, the stair-like morphology of the BSF, the structural high in the central part of the graben, and two minibasins flanking the structural high (Figures 5B and 5C) are well illustrated. Subsidence is controlled by dip-slip motion along the BSFs, which in turn are linked to strike-slip along the southern PBC. From the thickness of the sedimentary successions, we infer that this structure started to develop around the deposition of S-5 as younger sequences thin toward the uplifted structural high.

Seismic section Z-Z', transecting the plate boundary graben across the eastern portion of the NPB transfer zone, is shown in Figure 6. The raw seismic image (Figure 6A) reveals a structural depression bounded by a series of opposite-dipping fault scarps that curve (in plan view) and link with the bordering Pescadero and Atl transform farther to the NE. The scarps show little degradation, suggesting a recent origin (Figure 6B). This interpretation is also supported by the thin blanket of sediments lining the basin floor (Figures 6C and 9). The maximum thickness of the sedimentary cover is ~100 m vs. the ~1 km of sediments accumulated in the south graben. If we assume a constant sedimentation rate throughout the basin these successions should correspond to S-7 and S-8 in cross-sections X-X' and Y-Y' (Figures 4C and 5C). However, the sediments filling the central graben appear to be intercalated with a series of sharp, high-amplitude and high frequency reflectors intercalated with transparent layers not seen in the other cross-sections (Figures 5B and 8), suggesting poor lateral continuity.

4.3 Tectono-stratigraphic evolution of the PBC

A series of incremental cross-sectional restorations were constructed based on the interpretation of the seismic profile X-X' shown in Figure 4. This profile was selected because it is oriented sub-parallel to the maximum instantaneous stretching axis of the southern GoC (see Figure 3B) and contains the complete record of the stratigraphic evolution of the PBC. The restorations illustrate the Miocene-to-recent tectono-stratigraphic evolution of the PBC and depict variations in subsidence, uplift, sedimentation, and erosion as a function of strain and time. We distributed the linear extension calculated for the basin (see supplemental Figure S1 and Table S1) among all the paleo-sections, and assumed conservation of area, length, and layer thickness during their construction. For these assumptions to be valid, however, it is necessary that sediments and basement are incompressible and that rocks deform by brittle deformation and bending only.

In the tectono-stratigraphic model shown in Figure 7, the first two stages correspond to the initiation of continental rifting, around the middle Miocene (~10 Ma; Umhoefer et al., 2011; Umhoefer et al., 2018). At this time, a set of faults formed a semi graben with a westward polarity, which was infilled with the coarse-grain sequence S-1. In the restorations we have ignored the effects of pre-existing topography for simplicity but it is likely that the sediments were derived from local sources (Figure 3A). During the third and fourth stages (late Miocene, 7-8 Ma) a series of strike-slip faults, which progressively migrated towards the west, accommodated the extension and subsidence in the basin. Even though the Central Pescadero Transform acted as the master-bounding fault during much of the rifting evolution, by the late Miocene (~6 Ma) the main structures to the east also started to accommodate vertical deformation. Fault migration was accompanied by the onset of a transitional and continental shelf sedimentation environment with facies grading from sand to silt and mud (layer S-2 in Figure 7), followed immediately by the deposition of sediments from the first marine incursions S-3 (Umhoefer et al., 2007; Umhoefer, 2011; Umhoefer et al., 2018).

Observations of clinoforms in the seismic profile X-X' (Figure 4) suggest that during late Miocene (~6 Ma.), sedimentation was controlled by different episodes of marine regressions and transgressions (light tan sequence S-4 in Figure 4C). These sets also mark the beginning of the transtensional deformation, by which time 80% of the estimated extension (see Table S1 in the supplemental material) had been accommodated in the PCB, and the onset of the modern Pacific-North American plate boundary. This is a period of rapid subsidence characterized by the deposition of low-energy facies, and by the Pliocene (~2.6 Ma), the PBC became a deep-water basin in which the water depth exceeded 2000 meters (Umhoefer et al., 2018). Intrabasinal faults started to rotate, lessening their dip angles, accommodating more strain, while deep-marine low-energy sequences (sequence S-5 in Figure 7) continued to deposit. Finally, the current configuration is characterized by the propagation of low-angle transform faults converging towards the lower crust, suggesting the PBC is a crustal-scale negative flower structure, transitioning from narrow V-shaped grabens in the corners of the pull-apart basins, to more symmetric U-shaped grabens at the center of the stepovers. Finally, the present-day environment is that of a sediment-starved narrow basin being filled by hemipelagic sediments and intercalations of fine-grain facies (sequence S-7 in Figure 4C).

5. Discussion

5.1 Factors controlling basin geometry and evolution

This study provides insights into the geometry, structural evolution, internal structure and oblique rifting dynamics that led to the opening of the GoC. Moreover, our observations on the structural controls influencing the development and tectonic geomorphology of the PBC corroborate numerical and experimental models of pull-apart basin formation and evolution (e.g., Gölke et al., 1994; McClay & Dooley, 1995; Dooley & McClay, 1997; Rahe et al., 1998; Sims et al., 1999; Basile and Brun, 1999; Wu et al., 2009; Joshi and Hayashi, 2010; Corti & Dooley, 2015; van Wijk et al., 2017; Corti et al., 2020).

The seismic facies analysis and the series of restored sections (Figure 4) show that the PBC developed in a dynamic environment in which deformation shifted constantly through time and space. Sedimentation follows a stratigraphic succession observed in numerous rift basins in which a series of fluvial or shoreline sandstones are overlain by fine grained lacustrine successions or deep marine turbiditic deposits (e.g., Prosser, 1993; Lambiase, 1990). This 'rift-initiation' to 'rift-climax' transition, previously recognized in syn-rift stratigraphy, is the product of the onset of strong fault interaction and linkage accompanied by the rapid enlargement and slip localization onto major faults (Contreras et al., 1997; Contreras et al., 2000; Cowie et al., 2000). This development explains, in turn, observations in the seismic images such as the abandonment of faults in the early rifting stage and suggests that the increase in fault activity at ~7-6 Ma marks the time when deformation became localized onto a through-going fault, i.e., the bounding Central Pescadero Transform (Figure 7). However, in contrast to orthogonal rift system fault dynamics, the rift-initiation stage in the PBC likely corresponds to the development of Riedel shears and tensional fractures, structures often observed in strike-slip faulting analog models, whereas the rift-climax probably corresponds to their linkage into a PDZ (Tchalenko, 1970; Naylor, et al., 1986; Sims et al., 1999; Basile and Brun, 1999).

The seismic profiles also reveal that the basin geometry, as described by the length-to-width ratio (*l*/*w*), appears to be an evolving property rather than a feature of the system dictated by its initial conditions. Our structural analysis shows that the PBC became wider in the early stages of its development via westward fault migration and abandonment until the establishment of the Central Pescadero Transform at ~7 Ma (Figure 7). The northeastern Atl Transform appears to have undergone a similar development. The seismic line Z-Z' across the northeastern part of the PBC imaged a very young morphology and stratigraphy suggesting this part of the basin started to subside late in the history of the basin. This delay, in turn, indicates that the Atl Transform is either the result of NE fault activity migration or that it propagated laterally SE from the Farallon Basin. Regardless, the southern GoC rift system underwent a reorganization in transform faulting in the recent geologic past (~2-1 Ma).

5.2 Scaling relationships of the PBC and implications for continental rupture

Early models of pull-apart basin formation proposed that they evolve from incipient to extremely mature basins following a relatively clear deformation path (e.g., Mann et al., 1983; Dooley & McClay, 1997; Rahe, et al., 1998), and assumed fault growth as the leading cause influencing the basin's shape during different stages of evolution. Following these traditional models, the PBC and its associated basins can be classified as extremely evolved pull-apart basins according to their rhomboidal shape and fault overlap between their bordering transform faults. In addition, both basins are bounded by an array of oblique-normal faults (i.e., the BSFs) that are fully connected with the master transforms.

The PBC pull-apart basins also have been classified by their length-to-width ratio (Aydin & Nur, 1982; Dooley & McClay, 1997; Basile & Brun, 1999; Gürbüz, 2010). Using this approach, the SPB is a narrow basin (w=15.5 km) with an estimated fault overlap (l) of ~55 km between the master South and Central Pescadero transforms, which results in a l/w ratio of ~4. The NPB, in contrast, is nearly three times wider, and the fault overlap greatly exceeds that of the SPB by a factor of two, yielding a lower l/w of ~2.5. Thus, the length-to-width values for the SPB and NPB are in agreement with the most common range of l/w ratios determined directly for natural ($3 \leq l/w \leq 4$) (Aydin & Nur, 1982) and experimental ($2.2 \leq l/w \leq 3.8$) (Basile & Brun, 1999) pull-apart basins. However, the contrasting differences in scaling relationships and basin morphologies of the SPB and NPB suggest that they have followed distinct evolutionary trends throughout their short existence in the rapidly evolving GoC rift system (e.g., Umhoefer, 2011; Umhoefer et al., 2018).

A controlling factor that profoundly affects basin architecture and evolution is the initial step-over ratio of the master strike-slip faults configuration, (i.e., length vs. width of the strike-slip system) has only recently been recognized in experimental and field studies of pull-apart basins. It has been suggested that this ratio, which dictates the basin *l/w* ratio, plays a critical role in the extinction or longevity of pull-apart basins (van Wijk et al., 2017). Modeling results by van Wijk et al (2017) predict that pull-apart basins with larger *l/w* ratios with overlapping faults are more likely to progress to continental rupture. Such pull-apart geometries have been recognized in the southern GoC (e.g., van Wijk et al., 2017; this study), between Guaymas basin and the Alarcón Rise where continental rupture and then the onset of seafloor spreading began between 6.0 Ma and 3.7 Ma, respectively (Lizarralde, et al., 2007; Umhoefer, 2011; Sutherland et al., 2012; Umhoefer, et al., 2018 and references therein). In the PBC, seafloor spreading may have been delayed until ca. 2-1 Ma (Umhoefer, 2011; Umhoefer et al., 2020). Moreover, lava flows recently collected in the SPB and NPB (e.g., Paduan et al., 2019) suggest that the PBC evolved extremely rapid to full seafloor spreading.

Surface lava flows in the PBC are most conspicuous along the NE end of the NPB, where distributed outcrops of thinly sedimented young oceanic crust floor the narrow axial trough (Figures 6 and 9). Volcanic rocks on the SPB are, in contrast, restricted to the east side of a ~1 km wide sediment hill uplifted by intrusion of a sill. The hill sits on a fault-controlled ramp located west of the deepest portion of the basin (Paduan et al., 2019). These dramatic differences in volcanic activity and lava distribution in the SPB and NPB suggest distinct stages of basin evolution. The PBC pull-apart basin geometry consists of a master fault overlap that exceeds fault separation by a factor of ~2.5 and ~4 for the NPB and SPB, respectively. The length-to-width ratio is expected to increase with the age of the basins (e.g., van Wijk et al., 2017), yet the seemingly more mature, which shows more abundant near surface rift basalts, NPB yields a lower *l/w* ratio. To address this discrepancy requires further evaluation of the temporal and structural conditions that controlled pull-apart basin evolution of the PBC.

Previously, little was known about the initial conditions of the PBC. Our seismic facies analysis reveals that PBC pull-apart basins coexisted in a terrestrial environment since at least ca. 8 Ma, before the entire complex was flooded by marine waters between 8 and 7 Ma (Figure 7; see also Umhoefer et al., 2018 and references therein). Our palinspastic restorations and seismic survey also show that basin length is a function of the stretching associated with strike-slip displacement, and that increased displacement caused the width of the fault zone to increase, resulting in a wider pull-apart geometry (e.g., Gürbüz, 2010; van Wijk et al., 2017). Thus, our observations suggest that basin geometry is not only the result of initial conditions related to inheritance but also is an evolving property controlled by fault weakening processes. The estimated 2:1 ratio of fault overlap between the master strike-slip faults that bound the NPB and SPB, respectively, suggests that NPB stretched more over the same period of time. We hypothesize that this extension event was likely to occur in response to strain localization along the bordering master transforms which accelerated the rate of strike-slip displacement, leading the NPB to grow wider and also to achieve the geometry of an active spreading segment (Figure 9).

Simultaneously, the narrower SPB evolved less rapidly, reaching its present stretched-sigmoidal geometry characterized by a complex of sills and sediment cover exceeding ~50 m in thickness (e.g., Paduan et al., 2018). The lagging evolution of the SPB could result from a combination of geometrical and/or structural factors, including: 1) the initially close separation distance and the degree of fault underlap between the South and Central Pescadero strike-slip system, and/or 2) subtle changes in the azimuth of the Central Pescadero Transform fault, which could have promoted the formation of narrow transpressional fault zones that could lock and/or delay strike-slip displacement, resulting in a reduced rate of fault overlapping and pull-apart development. Evidence for the latter mechanism along the Central Pescadero Transform can be observed in the NE corner of the SPB (Figure 3A). There, the high-resolution bathymetry shows that a sinistral turn along the right-lateral Central Pescadero Transform is producing a contractional bend, characterized by an elongated marginal ridge. This bend is interpreted as a positive flower structure. In summary, the distinctive geometries and geological features characterizing the PBC reconcile that pull-apart basins do not necessarily follow a particular evolutionary path (Mann, et al., 1983). Instead their shape and structure appears to be primarily dictated by the initial geometry and behavior of the strike-slip system (e.g., Joshi and Hayashi, 2010; van Wijk et al., 2017).

5.3 Faulting patterns and structural elements evidencing transtensional deformation

The southern GoC contains a series of pull-apart basins with similar shapes and geometries, but radically different structures, faulting patterns, and/or morphological features. Despite their variability, analog simulations for oblique-related pull-apart basins agree remarkably well with the PBC basins (e.g., Wu et al., 2009). Wu et al. (2009) showed that pull-apart basins developed under transtension compared to pure strike-slip are: i) wider, ii) foster characteristic margins of en-echelon oblique-extensional faults, iii) form distinct narrow graben systems above the PDZs, iv) develop dual depocenters (i.e., mini basins) separated by a intra-basin structural high, and v) promote the earlier development of a strike-slip cross-basin fault system linking the offset PDZs. Regarding this last point, it should be noted that pull-apart basins are predicted to become extinct when an active cross-basin fault (CBF) system forms (e.g., Rahe et al., 1998; Sims et al., 1999; Wu et al., 2009; Corti & Dooley, 2015; Corti et al., 2020). Clearly, and for the various reasons that we discuss in the next section, CBFs in the PBC have not fully evolved to cut diagonally across the basin's floor to completely connect with the bounding PDZs.

Crosscutting relationships derived from the detailed mapping and analysis of the different fault systems in the PBC, show that the NW-striking CBFs propagating diagonally from the corners of the pull-apart basins are either connected or crosscut by the N-NE-striking BSFs with normal-slip kinematics (Figure 3A). This relationship clearly suggests that ongoing pull-apart rifting continues to dominate basin evolution, and that BSFs have overtaken and/or reduced the strike-slip rate of the CBFs, and thus inhibiting their complete development. This observation is further supported by the development of the narrow graben systems that characterize the plate boundary at the corners of the PBC (Figure 3A), where the obliquity of the BCFs with the bounding South and Central Pescadero, and Atl transforms varies between ~20º and ~28º, also consistent with experimental observations (e.g., Basile & Brun, 1999).

Van Wijk et al. (2017) proposed that elongated pull-apart basins with large length-to-width ratios (*l/w*) with overlapping master strike-slip faults are least likely to allow the full development of CBFs, and that pull-apart basins with this geometry are in turn the most prone to progress to continental rupture. We propose that this particular scenario is the one that applies to the PBC, as pull-apart basins here are characterized by high *l/w* ratios (see section 5.2). We further suggest that BCFs of the PBC initiated as en-echelon synthetic Riedel faults that propagated diagonally from each corner of the step-over, and terminate along-strike against progressively younger BSFs towards the central portions of the basins. Moreover, with progressive deformation along the divergent-wrench fault zone, the underdeveloped BCFs increasingly rotated clockwise around a vertical axis to acquire their present orientation. Basile & Brun (1999) compared BCFs with synthetic Riedel (R) faults, and suggested that the departure from the angle of 15^{o} expected from the Mohr-Coulomb rock failure theory, and the observed orientation of R faults in their model, was primarily a consequence of the interaction between strike-slip and divergent components resulting in a trend of the R faults rotating clockwise by the extensional component. Natural examples of basins developed in transtension, involving the development of synthetic R faults and crustal block rotations, include the North Aegean Trough and Sea of Marmara (McNeill et al., 2004 and references therein).

The Juno and Kai faults in the CPB and NPB, are examples of underdeveloped BCFs. The angle of these faults with the bounding Central Pescadero Transform is 20^{o} and 28^{o}, respectively, suggesting a magnitude of clockwise rotation between 5^{o} and 13^{o} of the northern half of the PBC. Elsewhere in the PBC, a number of BCFs with lesser angles with the transform boundaries are observed to control the subsidence along the inner (basin-side) faulted segments of the narrow graben systems that characterize the corners of the PBC pull-apart basins. From the surface geology, we interpret these plate-boundary graben systems as a series negative flower structures, characterized in cross-section by shallow synforms and concave upward strands of oblique-normal and/or synthetic Riedel faults merging at depth with a central subvertical strand (e.g., Naylor et al., 1986; Wu et al., 2009; Huang and Liu, 2017 and references therein). We propose that these oblique-extensional structures may have served as connections facilitating marine waters to breach and flood the pull-apart basins of the PBC during the early stages of development of the GoC seaway between 8 and 7 Ma (Umhoefer et al., 2018).

6. Conclusions

This study provides new insights into the geometry, structural symmetry, internal structure and oblique rifting processes leading to the development and evolution of the PBC in the southern GoC. On the basis of our analysis we conclude:

1. The Pescadero Basin Complex (PBC) comprises three distinctive rhombohedral-shaped pull-apart basins separated by short but highly overlapped transform faults. Basin geometry is strongly controlled by synthetic and antithetic strike-slip faults, whereas localized normal faulting and local oblique-slip along BSFs and secondary synthetic faults, respectively, accommodate basin subsidence.
2. Fundamental elements controlling basin architecture and evolution of the PBC include the geometric properties associated with (or inherited from) the initial configuration of the master strike-slip fault step over and fault dynamics, which may cause transients in fault activity and basin reconfigurations. Based on geometry and scaling relationships, the PBC and associated basins are extremely evolved pull-apart basins.
3. The distinctive geometries and geological features characterizing the PBC show that pull-apart basins do not necessarily follow a particular evolutionary path where the shape and structure are primarily dictated by the initial geometry and behavior of the strike-slip system. Seismic section analysis shows that the basin geometry, as described by the length-to-width ratio (*l*/*w*), is an evolving property rather than a feature of the system dictated by initial conditions.

4. Our structural analysis shows that the PBC and the northeastern PDZ became wider in the early stages of its development and that the northeastern part of the PBC has a young morphology and stratigraphy suggesting that this part of the basin started to subside at a late time in the history of the basin. This timeline suggests that the southern GoC rift system underwent reorganization in transform faults in the recent geologic past (~2-1 Ma).
5. Crosscutting relationships of the different fault systems in the PBC indicates that ongoing pull-apart rifting continues to dominate basin evolution, and that BSFs have overtaken and/or reduced the strike-slip rate of the CBFs, thus inhibiting their complete development.
6. We propose that the BCF's of the pull-apart basin comprising the PBC initiated as synthetic Riedel faults and with progressive deformation, rotated clockwise 5°-13° around a vertical axis to acquire their present orientation. BCFs with lower obliquities control the subsidence along the basin-side faulted segments of the narrow plate-boundary graben systems that characterize the corners of the PBC pull-apart basins. These narrow transtensional features may have served as connections facilitating marine waters to breach and flood the PBC during the early stages of formation of the GoC.

7. References

Abbott, P. L., & Smith, T. E. (1989). Sonora, Mexico, source for the Eocene Poway conglomerate of southern California. *Geology*, *17*(4), 329-332. https://doi.org/10.1130/0091-7613(1989)017<0329:SMSFTE>2.3.CO;2

Allmendinger, R.W., Cardozo, N. and Fisher, D.M. (2012). Structural Geology Algorithms: Vectors and Tensors. Cambridge University Press. 302 p. https://doi.org/10.1017/CBO9780511920202

Aragón-Arreola, M. and Martín-Barajas, A. (2007). Westward migration of extension in the northern Gulf of California, Mexico. *Geology*, *35*(6), 571-574. https://doi.org/10.1130/G23360A.1

Aranda-Gómez, J.J. y Pérez-Venzor, J.A. (1988). Estudio geológico de Punta Coyotes, Baja California Sur: Universidad Nacional Autónoma de México, Instituto de Geología, Revista, 7(1), 1-21.

Atwater, T. and Stock, J. (1998). Pacific-North America plate tectonics of the Neogene southwestern United States: an update. *International Geology Review*, *40*(5), 375-402. https://doi.org/10.1080/00206819809465216

Aydin, A. and Nur, A. (1982). Evolution of pull-apart basins and their scale independence. Tectonics 1:91–105. http://dx.doi.org/10.1029/TC001i001p00091.

Badley, M.E. (1985). Practical Seismic Interpretation: International Human Resources Development Corporation. Boston, MA, USA. 266 pp. ISBN:244-7-50680-857-9

Balestrieri, M.L., Ferrari, L., Bonini, M., Duque-Trujillo, J., Cerca, M., Moratti, G. and Corti, G. (2017). Onshore and offshore apatite fission-track dating from the southern Gulf of California: Insights into the time-space evolution of the rifting: Tectonophysics, 719, 148-161. https://doi.org/10.1016/j.tecto.2017.05.012

Basile, C., and Brun, J.P. (1999). Transtensional faulting patterns ranging from pull-apart basins to transform continental margins: An experimental investigation: Journal of Structural Geology, v. 21, p. 23–37, doi: 10.1016/S0191-8141(98)00094-7.

Bennett, S. E. K., Oskin, M. E. and Iriondo, A. (2013) Transtensional rifting in the proto-Gulf of California, near Bahía Kino, Sonora, México. *Geological Society of America Bulletin* 125:1752–1782. https://doi.org/10.1130/B30676.1

Bennett, S. E. and Oskin, M. E. (2014). Oblique rifting ruptures continents: Example from the Gulf of California shear zone. *Geology*, *42*(3), 215-218. https://doi.org/10.1130/G34904.1

Bennett, S. E., Oskin, M. E., Iriondo, A., & Kunk, M. J. (2016). Slip history of the La Cruz fault: Development of a late Miocene transform in response to increased rift obliquity in the northern Gulf of California. *Tectonophysics*, *693*, 409-435. https://doi.org/10.1016/j.tecto.2016.06.013

Bischoff, J.L., and Niemitz, J.W. (1980). Bathymetric maps of the Gulf of California. U.S. Geological Survey. https://doi.org/10.3133/i1244.

Bohannon, R.G., & Parsons, T. (1995). Tectonic implications of post–30 Ma Pacific and North American relative plate motions. *Geological Society of America Bulletin*, *107*(8), 937-959. https://doi.org/10.1130/0016-7606(1995)107<0937:TIOPMP>2.3.CO;2

Bot, A., Geoffroy, L., Authemayou, C., Bellon, H., Graindorge, D., and Pik, R. (2016). Miocene detachment faulting predating EPR propagation: Southern Baja California: Tectonics, 35(5), 1153-1176. https://doi.org/10.1002/2015TC004030

Brothers, D., Harding, A., González-Fernández, A., Holbrook, W.S., Kent, G., Driscoll, N., Fletcher, J., Lizarralde, D., Umhoefer, P. and Axen, G. (2012). Farallon slab detachment and deformation of the Magdalena Shelf, southern Baja California. *Geophysical Research Letters*, *39*(9). https://doi.org/10.1029/2011GL050828

Brune, S., Popov, A. A., and Sobolev, S. V. (2012). Modeling suggests that oblique extension facilitates rifting and continental break-up. *Journal of Geophysical Research: Solid Earth*, *117*(B8). https://doi.org/10.1029/2011JB008860

Brune, S., Williams, S. E., and Müller, R. D. (2018). Oblique rifting: the rule, not the exception. *Solid Earth*, *9*(5), 1187-1206. https://doi.org/10.5194/se-9-1187-2018

Cardozo, N. and Allmendinger, R.W. (2013). Spherical projections with OSXStereonet. *Computers & Geosciences*, *51*, pp.193-205. https://doi.org/10.1016/j.cageo.2012.07.021

Catuneanu, O. (2002). Sequence stratigraphy of clastic systems: concepts, merits, and pitfalls. *Journal of African Earth Sciences*, *35*(1), pp.1-43.https://doi.org/10.1016/S0899-5362(02)00004-0

Chopra, S., Marfurt, K.J. (2007). Seismic attributes for prospect identification and reservoir characterization. Tulsa, Oklahoma, U.S.A., Society of Exploration Geophysicists and European Association of Geoscientists and Engineers, 457 pp. https://doi.org/10.1190/1.9781560801900

Contreras, J., Scholz, C.H. and King, G.C. (1997). A model of rift basin evolution constrained by first-order stratigraphic observations. Journal of Geophysical Research: Solid Earth, 102(B4), p.7673-7690. https://doi.org/10.1029/96JB03832

Contreras, J., Anders, M.H., Scholz, C.H. (2000). Growth of a normal fault system: observations from the Lake Malawi basin of the east African rift. Journal of Structural Geology. Vol. 22, No.2 p. 159–168. https://doi.org/10.1016/S0191-8141(99)00157-1

Corti, G., and Dooley, T.P., (2015). Lithospheric-scale centrifuge models of pull-apart basins: Tectonophysics, v. 664, p. 154–163, https://doi.org/10.1016/j.tecto.2015.09.004.

Corti, G., Nencini, R., and Skyttä, P. (2020). Modelling the influence of pre-existing brittle fabrics on the development and architecture pull-apart basins: Journal of Structural Geology, vol. 131, https://doi.org/10.1016/j.jsg.2019.103937.

Cowie, P.A., Gupta, S. and Dawers, N.H. (2000). Implications of fault array evolution for synrift depocentre development: insights from a numerical fault growth model. *Basin Research*, *12*(3-4), pp.241-261.https://doi.org/10.1111/j.1365-2117.2000.00126.x

Darin, M. H., Bennett, S. E. K., Dorsey, R. J., Oskin, M. E., and Iriondo, A. (2016). Late Miocene extension in coastal Sonora, México: Implications for the evolution of dextral shear in the proto-Gulf of California oblique rift. *Tectonophysics*, *693*, 378-408. https://doi.org/10.1016/j.tecto.2016.04.038

DeMets, C. (1995). A reappraisal of seafloor spreading lineations in the Gulf of California: Implications for the transfer of Baja California to the Pacific plate and estimates of Pacific-North America motion. *Geophysical Research Letters*, *22*(24), 3545-3548. https://doi.org/10.1029/95GL03323

Díaz-Azpiroz, M., Brune, S., Leever, K. A., Fernández, C., and Czeck, D. M. (2016). Tectonics of oblique plate boundary systems. *Tectonophysics*, *693*, 165-170. https://doi.org/10.1016/j.tecto.2016.07.028

Dooley, T.P., McClay, K. (1997). Analog modeling of pull-apart basins. AAPG (Am. Assoc. Pet. Geol.) Bull. 81 (11), 1804–1826. https://doi.org/10.1306/3B05C636-172A-11D7-8645000102C1865D

Duque-Trujillo, J., Ferrari, L., Orozco-Esquivel, T., López-Martínez, M., Lonsdale, P., Bryan, S. E., Kluesner, J., Piñero-Lajas, D., and Solari, L. (2015). Timing of rifting in the southern Gulf of California and its conjugate margins: Insights from the plutonic record. *Geological Society of America Bulletin*, *127*(5-6), 702-736. https://doi.org/10.1130/B31008.1

Dziewonski, A.M., Chou, T.A. and Woodhouse, J.H. (1981). Determination of earthquake source parameters from waveform data for studies of global and regional seismicity. *Journal of Geophysical Research: Solid Earth*, *86*(B4), pp.2825-2852.https://doi.org/10.1029/JB086iB04p02825

Emery, D., and Myers, K. (1996). Sequence Stratigraphy, Blackwells. Oxford, 297 pp. ISBN 0 632 03706 7

Ekström, G., Nettles, M. and Dziewoński, A.M. (2012). The global CMT project 2004–2010: Centroid-moment tensors for 13,017 earthquakes. *Physics of the Earth and Planetary Interiors*, *200*, pp.1-9.https://doi.org/10.1016/j.pepi.2012.04.002

Ferrari, L., López-Martínez, M., Orozco-Esquivel, T., Bryan, S.E., Duque-Trujillo, J., Lonsdale, P. and Solari, L. (2013). Late Oligocene to Middle Miocene rifting and synextensional magmatism in the southwestern Sierra Madre Occidental, Mexico: The beginning of the Gulf of California rift. *Geosphere*, *9*(5), pp.1161-1200.https://doi.org/10.1130/GES00925.1

Fletcher, J.M., Pérez-Venzor, J.A., Gonzáles-Barba, G., & Aranda-Gómez, J.J. (2003). Ridge-trench interactions and the ongoing capture of the Baja California microplate—New insights from the southern Gulf extensional province, en 99th Geological Society of America Cordilleran Section Annual Meeting, Geologic Transects across Cordilleran México (abstract), Guidebook for Field Trips, 13-31.

Fletcher, J. M., Grove, M., Kimbrough, D., Lovera, O. and Gehrels, G. E. (2007). Ridge-trench interactions and the Neogene tectonic evolution of the Magdalena shelf and southern Gulf of California: Insights from detrital zircon U-Pb ages from the Magdalena fan and adjacent areas. *Geological Society of America Bulletin*, *119*(11-12), 1313-1336. https://doi.org/10.1130/B26067.1

Fossen, H., and Tikoff, B. (1993). The deformation matrix for simultaneous simple shearing, pure shearing and volume change, and its application to transpression-transtension tectonics. *Journal of Structural Geology*, *15*(3-5), 413-422. https://doi.org/10.1016/0191-8141(93)90137-Y

Gans, P. B. (1997). Large-magnitude Oligo-Miocene extension in southern Sonora: Implications for the tectonic evolution of northwest Mexico. *Tectonics*, *16*(3), 388-408. https://doi.org/10.1029/97TC00496

Gastil, R. G., Lemone, D. V. and Stewart, W. J. (1973). Permian fusulinids from near San Felipe, Baja California. *The American Association of Petroleum Geologists Bulletin*, *57*(4), 746-747. https://doi.org/10.1306/819A431E-16C5-11D7-8645000102C1865D

Gölke, M., Cloetingh, S. and Fuch, K. (1994). Finite element modeling of pull-apart basin formation. Tectonophysics 240, p. 45–57. http://dx.doi.org/10.1016/0040-1951(94)90263-1.

Gürbüz, A. (2010). Geometric characteristics of pull-apart basins. *Lithosphere*, *2*(3), pp.199-206. https://doi.org/10.1130/L36.1

Harding, T. P. (1990). Identification of wrench faults using subsurface structural data: criteria and pitfalls (1). *The American Association of Petroleum Geologists Bulletin*, *74*(10), 1590-1609. https://doi.org/10.1306/0C9B2533-1710-11D7-8645000102C1865D

Henry, C.D. and Aranda-Gomez, J.J. (2000). Plate interactions control middle–late Miocene, proto-Gulf and Basin and Range extension in the southern Basin and Range. *Tectonophysics*, *318*(1-4), pp.1-26.https://doi.org/10.1016/S0040-1951(99)00304-2

Huang, L., & Liu, C.-y. (2017). Three types of flower structures in a divergent-wrench fault zone. Journal of Geophysical Research: Solid Earth, 122, 10,478–10,497. https://doi.org/10.1002/ 2017JB014675

Joshi, G.R., and Hayashi, D. (2010). Finite element modelling of the pull-apart formation: implication for tectonics of Bengo Co pull-apart basin, southern Tibet: Natural Science, v. 02, p. 654–666, doi: 10.4236/ns.2010.26082.

Lambiase, J.J. (1990). A model for tectonic control of lacustrine stratigraphic sequences in continental Rift Basins: Chapter 16. In lacustrine exploration: Case studies and Modern Analogs, edited by B. Katz AAPG. Mem., 50, 265-276.

Lines, L. R. and Newrick, R. T. (2004). *Fundamentals of geophysical interpretation*. Society of Exploration Geophysicists. Geophysical Monograph Series no. 13. 269 pp. https://doi.org/10.1190/1.9781560801726

Lizarralde, D., Axen, G. J., Brown, H. E., Fletcher, J. M., González-Fernández, A., Harding, A. J., Holbrook, W.S., Kent, G.M., Paramo, P., Sutherland, F. and Umhoefer, P. J. (2007). Variation in styles of rifting in the Gulf of California. *Nature*, *448*(7152), 466. https://doi.org/10.1038/nature06035

Lonsdale, P. (1989). Geology and tectonic history of the Gulf of California, in *The Eastern Pacific Ocean and Hawaii*, D. Hussong, E. L. Winterer, and R. W. Decker (Editors), The Geology of North America, Vol. N, Geological Society of America, Boulder, Colorado, 499–521. https://doi.org/10.1130/dnag-gna-n.499

Macias-Iñiguez, I., Yarbuh, I., Spelz-Madero, R., González-Fernández, A., Fletcher, J. M., Contreras, J., Ramírez-Zerpa, N., Santa Rosa del Río, M.A. y Guardado-France, R. (2019). Modo de extensión de la corteza y formación del Sistema Extensional de Cerralvo, sur del Golfo de California, a partir de datos de reflexión sísmica en 2D. Revista Mexicana de Ciencias Geológicas, 36(3), 334-347. https://doi.org/10.22201/cgeo.20072902e.2019.3.1352

Mann, P., Hempton, M.R., Bradley, D.C., Burke, K. (1983). Development of pull-apart basins. *Journal of Geology*, 91, 529–554. https://doi.org/10.1086/628803

Marrett, R. and Allmendinger, R.W. (1990). Kinematic analysis of fault-slip data. *Journal of structural geology*, *12*(8), pp. 973-986.https://doi.org/10.1016/0191-8141(90)90093-E

McClay, K. and Dooley, T. (1995). Analogue models of pull-apart basins: *Geology*, v. 23, p. 711–714, https://doi.org/10.1130/0091-7613

McQuarrie, N. and Wernicke, B.P. (2005). An animated tectonic reconstruction of southwestern North America since 36 Ma. Geosphere, 1(3), pp. 147-172, https://doi: 10.1130/GES00016.1

McNeill, L.C., Mille, A., Minshull, T.A., Bull, J.M., Kenyon, N.H., Ivanov, M., 2004. Extension of the North Anatolian Fault into the North Aegean Trough: Evidence for transtension, strain partitioning, and analogues for Sea of Marmara basin models. Tectonics 23, 1–12. doi:10.1029/2002TC001490

Montrella, J.J. (2004). Geology of Isla Cerralvo, Baja California Sur, Mexico: San Diego State University, Department of Geological Sciences, Master of Science Thesis. 125 pp. http://hdl.handle.net/20.500.11929/sdsu:173

Naylor, M.A., Mandl, G., and Supesteijn, C.H.K. (1986). Fault geometries in basement-induced wrench faulting under different initial stress states: Journal of Structural Geology, v. 8, p. 737–752, doi: https://doi.org/10.1016/0191-8141(86)90022-2.

Negrete-Aranda, R., Contreras, J. and Spelz, R.M. (2013). Viscous dissipation, slab melting, and post-subduction volcanism in south-central Baja California, Mexico: Geosphere, v. 9, p. 1714–1728, doi: doi: 10.1130/GES00901.1.

Negrete-Aranda, R., Neumann, F., Contreras, J., Harris, R.N., Spelz, R.M., Zierenberg, R. and Caress, D.W. (2021). Transport of Heat by Hydrothermal Circulation in a Young Rift Setting: Observations From the Auka and JaichMaa Ja'ag' Vent Field in the Pescadero Basin, Southern Gulf of California: Journal of Geophysical Research: Solid Earth, v. 126, p. 1–20, doi: 10.1029/2021JB022300.

Oskin, M., Stock, J. and Martín-Barajas, A. (2001). Rapid localization of Pacific–North America plate motion in the Gulf of California. *Geology*, *29*(5), 459-462. https://doi.org/10.1130/0091-7613(2001)029<0459:RLOPNA>2.0.CO;2

Paduan, J.B., Zierenberg, R.A., Clague, D.A., Spelz, R.M., Caress, D.W., Troni, G., Thomas, H., Glessner, J., Lilley, M.D., Lorenson, T., Lupton, J., Neumann, F., Santa Rosa del Rio, M.A. and Wheat, C.G. (2018). Discovery of hydrothermal vent fields on Alarcón Rise and in Southern Pescadero Basin, Gulf of California. *Geochemistry, Geophysics, Geosystems*, *19*(12), pp.4788 4819. https://doi.org/10.1029/2018gc007771.

Paduan, J.B., Zierenberg, R.A., Caress, D.W., Spelz, R.M., Clague, D.A., Walker, S.L., Ramiírez-Zerpa, N. (2019). Mapping Pescadero Basin Hydrothermal Vent Fields at Multiple Scales. Abstract V33E-0235 presented at the Fall AGU Meeting, San Francisco, CA, December 9-13.

Páramo, P., Holbrook, W.S., Brown, H.E., Lizarralde, D., Fletcher, J., Umhoefer, P., Kent, G., Harding, A., Gonzalez, A. and Axen, G. (2008). Seismic structure of the southern Gulf of California from Los Cabos block to the East Pacific Rise. *Journal of Geophysical Research: Solid Earth*, *113*(B3). https://doi.org/10.1029/2007JB005113

Persaud, P., Stock, J. M., Steckler, M. S., Martín-Barajas, A., Diebold, J. B., González-Fernández, A. and Mountain, G. S. (2003). Active deformation and shallow structure of the Wagner, Consag, and Delfin basins, northern Gulf of California, Mexico. *Journal of Geophysical Research: Solid Earth*, *108*(B7). https://doi.org/10.1029/2002JB001937

Persaud, P., Tan, E., Contreras, J., and Lavier, L. (2017). A bottom-driven mechanism for distributed faulting in the Gulf of California rift: Tectonophysics, v. 719–720, p. 51–65 http://dx.doi.org/10.1016/j.tecto.2016.11.024.

Plattner, C., Malservisi, R., Dixon, T. H., LaFemina, P., Sella, G. F., Fletcher, J., & Suarez-Vidal, F. (2007). New constraints on relative motion between the Pacific plate and Baja California microplate (Mexico) from GPS measurements. *Geophysical Journal International*, *170*(3), 1373-1380. https://doi.org/10.1111/j.1365-246X.2007.03494.x

Prosser, S. (1993). Rift-related linked depositional systems and their seismic expression, in Tectonics and Seismic Sequence Stratigraphy, edited by G. D. Williams and A. Dobb, Geological Society Special Publication, 71, 35-66. . https://doi.org/10.1144/GSL.SP.1993.071.01.03

Rahe, B., Ferrill, D.A., and Morris, A.P. (1998). Physical analog modeling of pull-apart basin evolution: *Tectonophysics*, v. 285, p. 21–40, https://doi.org/10.1016/S0040-1951(97)00193-5

Richard, P. and Cobbold, P. (1990). Experimental insights into partitioning fault motions in continental convergent wrench zones, *Annales Tectonicae*. Vol 4, 1990, pp. 35-44. ISSN 0394-5596

Schaaf, P., Boehnel, H. and Perez-Venzor, J.A. (2000). Pre-Miocene palaeogeography of the Los Cabos Block, Baja California Sur; Geochronological and palaeomagnetic constraints: Tectonophysics, 318, 53-69. https://doi.org/10.1016/S0040-1951(99)00306-6

Seiler, C., Fletcher, J.M., Quigley, M.C., Gleadow, A.J.W. and Kohn, B.P. (2010). Neogene structural evolution of the Sierra San Felipe, Baja California: evidence for proto-gulf transtension in the Gulf Extensional Province? Tectonophysics 488, 87–109. http://doi:10.1016/j.tecto.2009.09.026

Sheriff, R.E. and Geldart, L.P. (1995). Exploration Seismology (2nd ed.). Cambridge University Press. ISBN: 9781139168359 https://doi.org/10.1017/CBO9781139168359

Sims, D., Ferrill, D.A. and Stamatakos, J.A. (1999). Role of a ductile decollement in the development of pull-apart basins: Experimental results and natural examples. *Journal of Structural Geology*, *21*(5), pp.533-554. https://doi.org/10.1016/S0191-8141(99)00010-3

Spencer, J. E. and Normark, W. R. (1979). Tosco-Abreojos fault zone: A Neogene transform plate boundary within the Pacific margin of southern Baja California, Mexico. *Geology*, *7*(11), 554-557. https://doi.org/10.1130/0091-7613(1979)7<554:TFZANT>2.0.CO;2

Stock, J. M. and Hodges, K. V. (1989). Pre-Pliocene extension around the Gulf of California and the transfer of Baja California to the Pacific plate. *Tectonics*, *8*(1), 99-115. https://doi.org/10.1029/TC008i001p00099

Stockwell Jr, J. W. (1999). The CWP/SU: seismic Un∗ x package. *Computers & Geosciences*, *25*(4), 415-419. https://doi.org/10.1016/S0098-3004(98)00145-9

Sutherland, F. H., Kent, G. M., Harding, A. J., Umhoefer, P. J., Driscoll, N. W., Lizarralde, D., Fletcher, J.M., Axen, J.G., Holbrook, W.S., González-Fernández, A. and Lonsdale, P. (2012). Middle Miocene to early Pliocene oblique extension in the southern Gulf of California. *Geosphere*, *8*(4), 752-770. https://doi.org/10.1130/GES00770.1

Tchalenko, J.S. (1970). Similarities between shear zones of different magnitudes: Bulletin of the Geological Society of America, v. 81, p. 1625–1640, doi: 10.1130/0016-7606(1970)81[1625:SBSZOD]2.0.CO;2.

Tron, V. and Brun, J.P. (1991). Experiments on oblique rifting in brittle-ductile systems. *Tectonophysics*, *188*(1-2), pp.71-84. https://doi.org/10.1016/0040-1951(91)90315-J

Umhoefer, P. J., Schwennicke, T., Del Margo, M. T., Ruiz-Geraldo, G., Ingle Jr, J. C., and McIntosh, W. (2007). Transtensional fault-termination basins: an important basin type illustrated by the Pliocene San Jose Island basin and related basins in the southern Gulf of California, Mexico. *Basin Research*, *19*(2), 297-322. https://doi.org/10.1111/j.1365-2117.2007.00323.x

Umhoefer, P. J. (2011). Why did the Southern Gulf of California rupture so rapidly? —Oblique divergence across hot, weak lithosphere along a tectonically active margin. *GSA Today*, *21*(11), 4-10. https://doi.org/10.1130/G133A.1.

Umhoefer, P. J., Darin, M. H., Bennett, S. E. K., Skinner, L. A., Dorsey, R. J., and Oskin, M. E. (2018). Breaching of strike-slip faults and successive flooding of pull-apart basins to form the Gulf of California seaway from ca. 8–6 Ma. *Geology*, *46*(8), 695-698. https://doi.org/10.1130/G40242.1

Umhoefer, P.J., Plattner, C., and Malservisi, R. (2020). Quantifying rates of “rifting while drifting” in the southern Gulf of California: The role of the southern Baja California microplate and its eastern boundary zone: Lithosphere, v. 12, p. 122–132. https://doi.org/10.1130/L1132.1

van Wijk, J., Axen, G., and Abera, R. (2017). Initiation, evolution and extinction of pull-apart basins: Implications for opening of the Gulf of California. *Tectonophysics*, *719*, 37-50. https://doi.org/10.1016/j.tecto.2017.04.019

Withjack, M. O. and Jamison, W. R. (1986). Deformation produced by oblique rifting. *Tectonophysics*, *126*(2-4), 99-124. https://doi.org/10.1016/0040-1951(86)90222-2

Wu, J.E., McClay, K., Whitehouse, P., and Dooley, T. (2009). 4D analogue modelling of transtensional pull-apart basins: Marine and Petroleum Geology, v. 26, p. 1608–1623, https://doi.org/10.1016/j.marpetgeo.2008.06.007.

Yilmaz, Ö. (2001). Seismic data analysis: Processing, inversion, and interpretation of seismic data, vol. 1, Society of Exploration Geophysicists, Tulsa, 2027 pp. ISBN: 1560800984

Zwaan, F., Schreurs, G., Naliboff, J. and Buiter, S.J. (2016). Insights into the effects of oblique extension on continental rift interaction from 3D analogue and numerical models. *Tectonophysics*, *693*, p. 239-260. https://doi.org/10.1016/j.tecto.2016.02.036

8. Acknowledgments

The authors wish to thank Andres Folguera, as well as another anonymous reviewer, for their valuable comments which substantially improved the content of this manuscript. We also thank the Schmidt Ocean Institute and the entire crew of the R/V Falkor (classic) for their support during expedition FK181031, particularly to the Lead Tech, Leighton Rolley, and the MTs John Fulmer and Deb Smith. We also thank Jennifer B. Paduan from the Monterey Bay Aquarium Research Institute (MBARI), for her support in processing the bathymetric data. Finally to Miguel Tellez-Duarte for his unconditional support throughout these years. Juan Contreras and Raquel Negrete-Aranda acknowledge the support from CICESE's internal project 644143 and 644165, respectively.

Figure captions

Figure 1. Regional tectonic map of the Baja California microplate (BCM) and the Gulf Extensional Province (yellow area). Major extension in the GEP initiated following the cessation of subduction of the Farallon plate west of Baja ca. ~12.5 Ma (black dashed lines denote the paleo-trench, abandoned spreading ridges, and the partially subducted Farallon-derived Guadalupe and Magdalena microplates captured by the Pacific plate). Purple dashed lines represent the extent of the northwestern portion of the Sierra Madre Occidental (SMO). Other abbreviations: EPR = East Pacific Rise; TF = Tosco fault; SM-SLF = Santa Margarita-San Lázaro faults, AF = Abreojos fault; GN = Guerrero Negro fault; OL = Ojo de Liebre fault; C = Cedros fault; SC-SI = Santa Catalina-San Isidro faults. Base map downloaded from GeoMapApp (http://www.GeoMapApp.org).

Figure 2. Seismotectonic map of the southern Gulf of California (GoC) showing major fault systems that accommodate shear along the margins of the Baja California microplate (BCM). Faults are color coded on the basis of their activity, kinematics and composition of the crust involved during faulting (after Fletcher et al., 2007 and Duque-Trujillo et al., 2015). Distribution of modern seismicity for events of magnitude M≥4 is shown (inset). Abbreviations: SPB = South Pescadero Basin, NPB = North Pescadero Basin, CPT = Central Pescadero transform. Bathymetry base map and seismic data (1971 to 2020) from the GeoMapApp catalog (http://www.GeoMapApp.org).

Figure 3. Structural and seismotectonic map of the Pescadero Basin Complex (PBC). Multi-beam bathymetry (40-m resolution) is superimposed over faded GMRT bathymetry from GeoMapApp. A) Structural map showing the geometry and 2D architecture of the pull-apart basins comprising the PBC. Abbreviations: PDZ = Principal displacement zone; SPB = South Pescadero Basin; CPB = Central Pescadero Basin; NPB = North Pescadero Basin. The calculated length-to-width ratio for each basin is indicated in parenthesis (see text for details). B) Seismotectonic map of the PBC showing the distribution

of focal mechanisms for events with magnitude $M_w \geq 4.7$ (n=57). C) Fault plane solutions (shown with a heavier line weight) were selected on the basis of geologic criteria and proximity to known faults. Equal-area stereo plots show fault planes and slip vectors (lower left) and orientation of the local principal stretching axes (lower right). The maximum instantaneous stretching axis (S1) is given by the eigenvector (red squares) with the highest eigenvalue: 5.8º (sub-horizontal) towards 266.4º. Notice the sub parallelism between S1 and seismic section X-X'. The best-fit plane, containing the two eigenvectors with the largest eigenvalues (great circle in red), dips 25.5º towards 188.6º. Kamb contour interval is 2σ, and significance level is 3σ. Statistical analyses for the orientation of linear data were calculated using OSXStereoplot v. 2.4 (Marrett & Allmendinger, 1990; Allmendinger et al., 2012; Cardozo & Allmendinger, 2013). Focal mechanisms are from the CMT solution (e.g., Dziewonsky et al., 1981; Ekström et al., 2012) from 1981 to 2019. D) Map view time frames showing the regional evolution of rift obliquity along the Gulf of California rift system for the last 8 Ma. Rift obliquity is measured as the angle α' spanned by the Pacific plate displacement vector (black arrow) and the rift trend normal (e.g., Brune et al., 2018). Rift trend (330º) is the average orientation of the Pacific-North America at 8 Ma (e.g., Darin et al., 2016 and references therein), and is assumed constant in all frames. Displacement vectors are from Atwater & Stock, 1998. The component of trantension is given by the angle α spanned by the rift trend and the Pacific plate displacement vector (see text for details).

Figure 4. Seismic profile X-X'. A) Raw seismic image; B) Structural and stratigraphic interpretation. The section consists of 15 seismic faults (black lines) with dip angles ranging between 20º and 81º (see Table S1). Dashed lines represent the horizontal and vertical components of deformation accommodated by each individual fault. Palinspastic restoration indicates a minimum of 22.5 km of extension sub-perpendicular to the gulf-axis system (see supplemental information S1); C) Cartoon showing the integrated representation of the interpreted seismic cross sections. Color-coded lines (L0 through L6) represent the stratigraphic boundaries of syn-kinematic sedimentary infill sequences, S1 through S7. L-0

represents the unconformity between the acoustic basement and syn-kinematic sediment sequences, while L1 represents the disconformity between terrestrial (S1) and marine sedimentary deposits (S2 through S7; see text). Intersection with the seismic line Y-Y' is indicated. Abbreviations: SC-FZ = Santa Cruz fault zone; CPT = Central Pescadero Transform; BSF = Basin sidewalk fault.

Figure 5. Seismic reflection profile Y-Y'. A) Raw seismic image; B) Structural and stratigraphic interpretation showing the series of ramps and basin sidewalk faults (black lines) that bound the opposite ends of the basins, and the central structural high separating the basin's depocenters; C) Cartoon showing the integrated representation of the interpreted seismic cross section. Color-coded lines (L0 through L7) represent the stratigraphic boundaries of syn-kinematic sedimentary infill sequences, S1 through S8 shown in Figure 5c. L-0 represents the unconformity between the acoustic basement and syn-kinematic sediment sequences, while L1 represents the disconformity between terrestrial (S1) and marine sedimentary deposits (S2 through S8; see text). Dashed box shows the location of Figure 8. Intersection with the seismic line X-X' is indicated. Other abbreviations: BSF = Basin sidewalk fault; NPB = North Pescadero Basin; CPB = Central Pescadero Basin.

Figure 6. Seismic reflection profile Z-Z'. A) Raw seismic image. B) Structural interpretation showing the asymmetric geometry of the basin. The NW side is characterized by a series of poorly eroded ramps and fault scarps produced by slip along the traversing basin sidewalk faults (BSFs; black lines). Red areas located within the innermost younger ramps, and at the surface of the axial graben, represent strong seismic reflectors that are interpreted as lava flows. Dashed box represents the location of Figure 9. C) Cartoon showing the integrated representation of the interpreted seismic cross section. Note the progressively thinner deposits of syn-tectonic sediments (shown in yellow) towards the center of the axial graben.

Figure 7. Conceptual model of the shallow tectonostratigraphic evolution of the northern Pescadero Basin Complex (PBC), based on the interpretation and finite strain analysis of the seismic profile X-X' (see the supplemental material that accompanies this paper). Discontinuous black lines are the original position of the faulting system. Each stage describes a temporal evolution of the PBC in terms of extension, subsidence, and sedimentation. The final stage (0 Ma) is shown as in Figure 4C. The Basement layer (gray color) has an arbitrary thickness and represents the meta-volcanic and meta-sedimentary rocks deposited before the opening of the PBC. The S-1 sequence represents sediments deposited during the rift's initial stage and is considered as pre-tectonic sedimentation in a terrestrial environment. S-2 and S-3 sequences represent sedimentation in transitional-to-continental shelf environments during the early marine incursions into the gulf. S-4, S-5, S-6, and S-7 represent high cyclicity sequences deposited in shallow and deep marine environments (see text for details).

Figure 8. Close up image of the west-central portion of the seismic profile Y-Y' (black dotted square in Figure 5B), showing the structure of the wider SW portion of the northern Pescadero axial graben. A) Raw seismic section image. B) Structural and stratigraphic interpretation. C) Cartoon showing the integrated interpretation of the seismic profile. Note that sediments filling the central graben are interstratified with a series of sharp, high-amplitude and high frequency reflectors intercalated with transparent layers. Sharp reflectors are interpreted as shallow (~100 m) hypabyssal magma bodies (saucer-shaped sills), whereas the transparent layers (black dotted lines in B and C) are interpreted as fluid-saturated sediments and/or zones of advective flow connecting with potential hydrothermal mounds sitting on the basin's sedimented floor.

Figure 9. Close-up image of the west-central part of seismic profile Z-Z' (black dotted square in Figure 6B), showing the axial graben of Northern Pescadero Basin. A) Raw seismic section image. B) Structural and stratigraphic interpretation. C) Cartoon showing the integrated interpretation of the seismic cross-section. The thin blanket of sediments lining the basin floor and the poorly degraded array of fault scarps

on the NW margin of the axial graben suggest a recent origin. The series of sharp, high-amplitude and high frequency reflectors intercalated with sediments towards the top of the innermost bounding ramps and on the bottom of the axial graben, are interpreted as lava flows related to active seafloor spreading (see text for details).

Figure 1

Click here to access/download;Figure;Figure_1.pdf

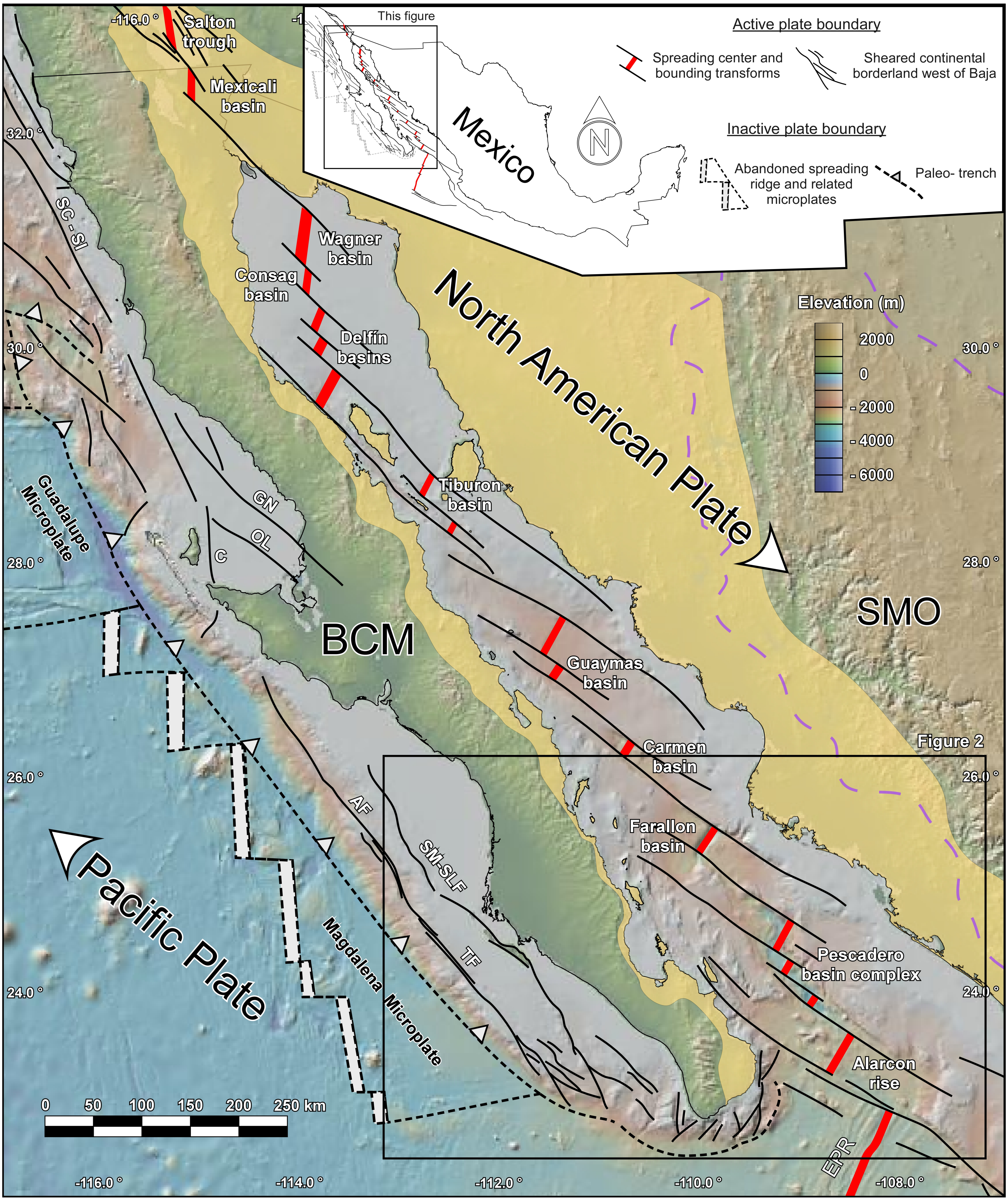

Figure 2 Click here to access/download;Figure;Figure_2.pdf

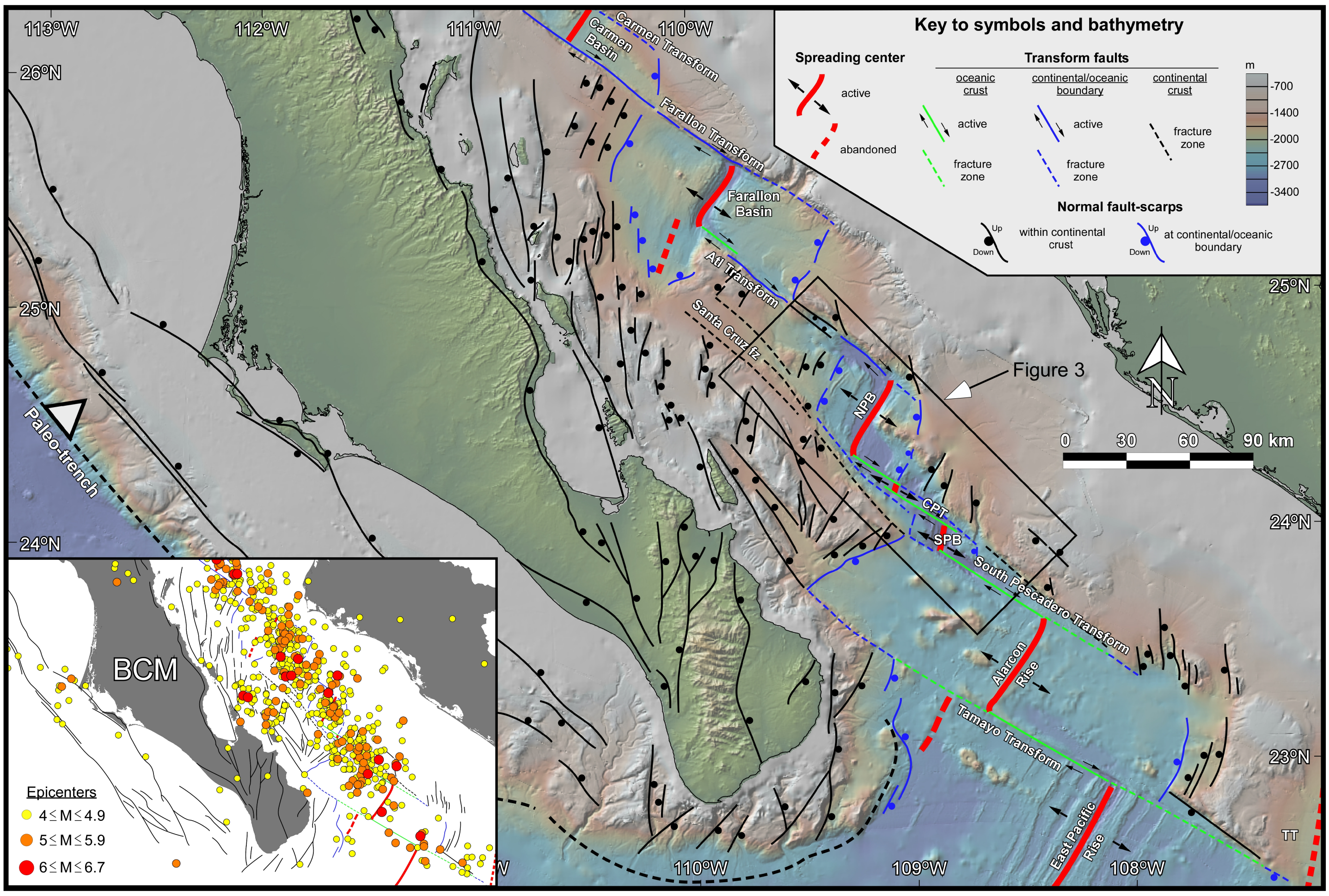

Figure 3 Click here to access/download;Figure;Figure_3.pdf

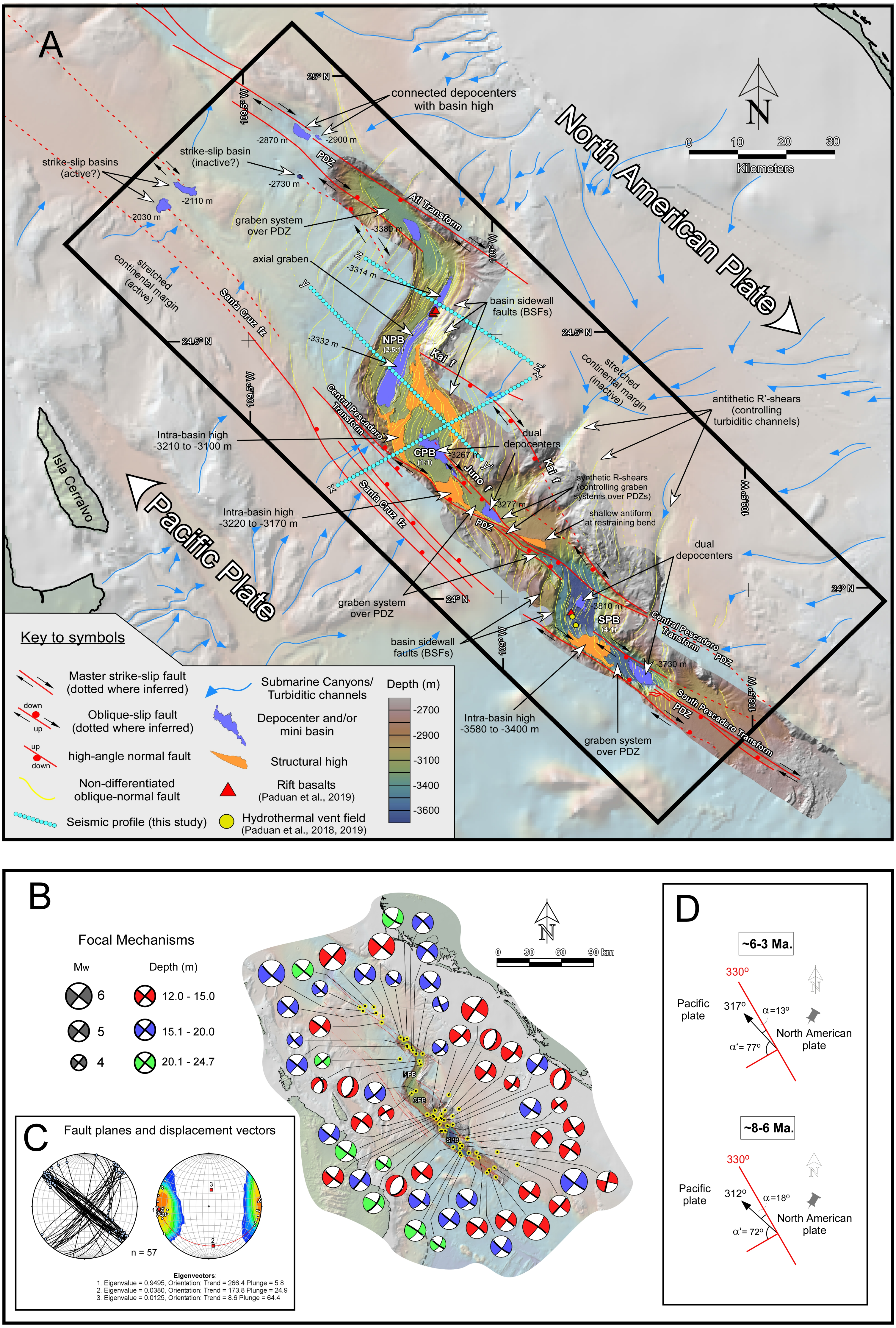

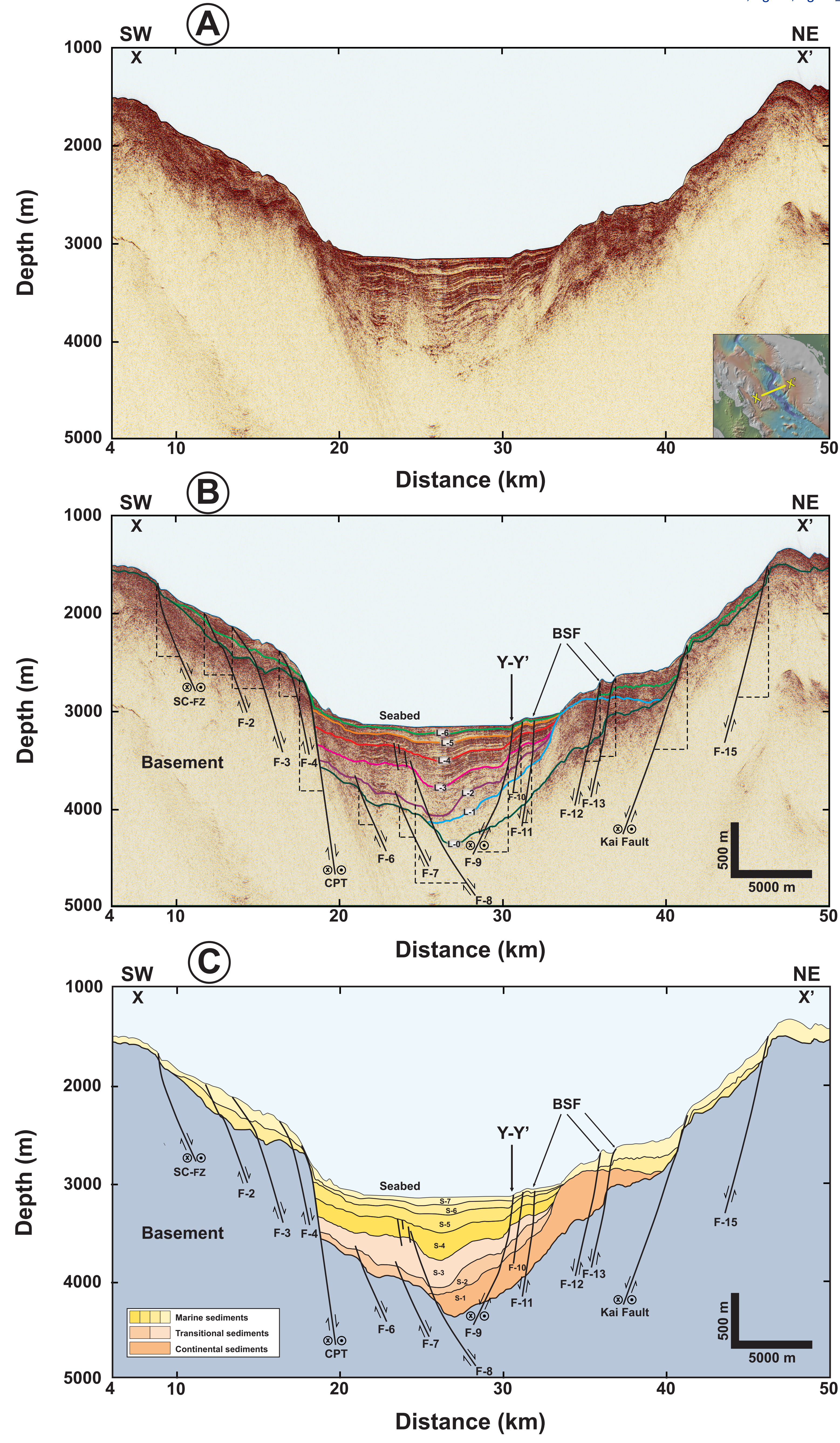
A
SW
X
NE
X'
Depth (m)
1000
2000
3000
4000
5000
Distance (km)
4
10
20
30
40
50
B
Seabed
Basement
SC-FZ
F-2
F-3
F-4
F-6
F-7
F-8
F-9
F-10
F-11
F-12
F-13
F-15
CPT
Kai Fault
BSF
Y-Y'
L-0
L-1
L-2
L-3
L-4
L-5
L-6
500 m
5000 m
C
S-1
S-2
S-3
S-4
S-5
S-6
S-7
Marine sediments
Transitional sediments
Continental sediments

Figure 5

Click here to access/download;Figure;Figure_5.pdf

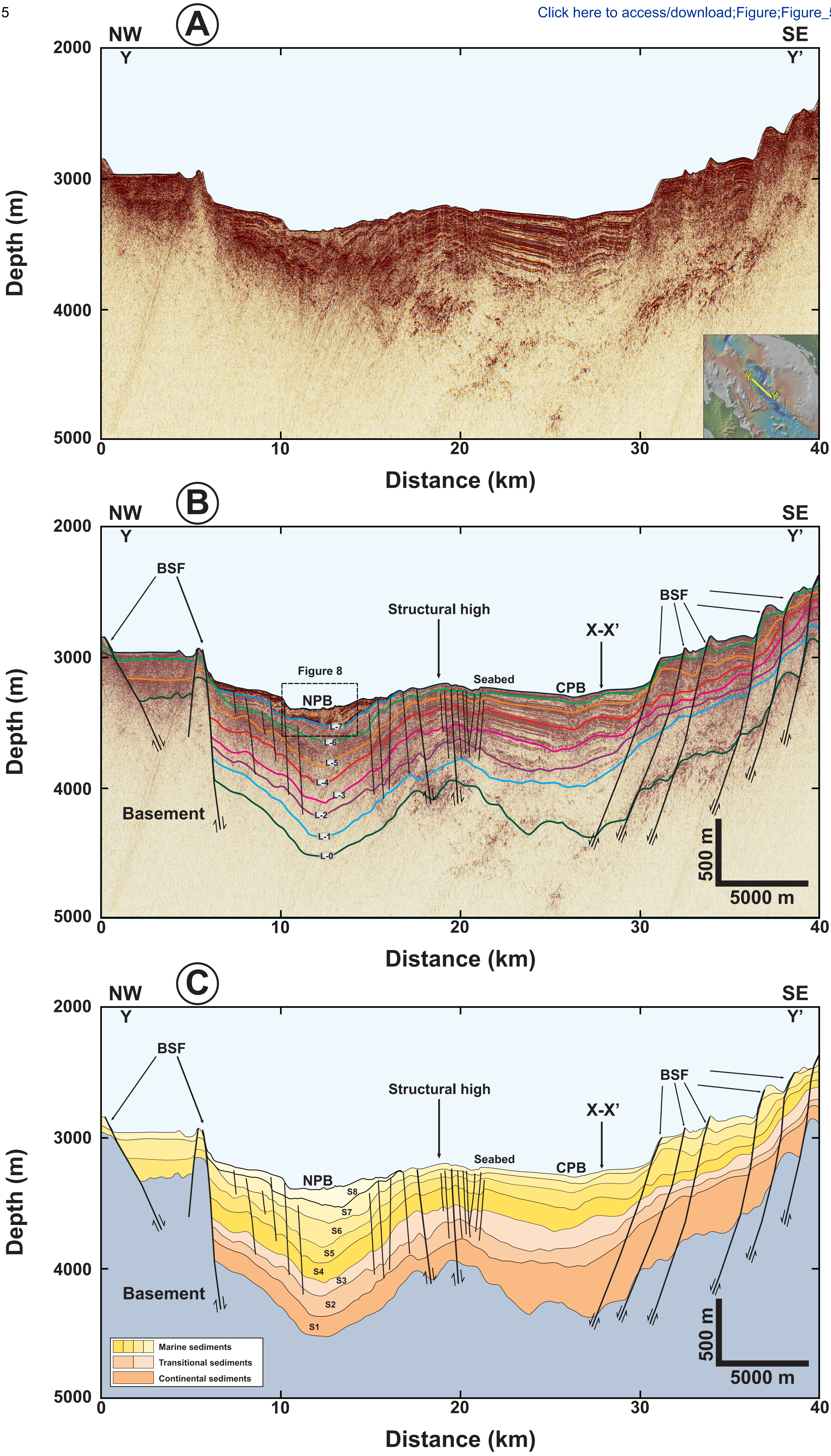

Figure 6

Click here to access/download;Figure;Figure_6.pdf

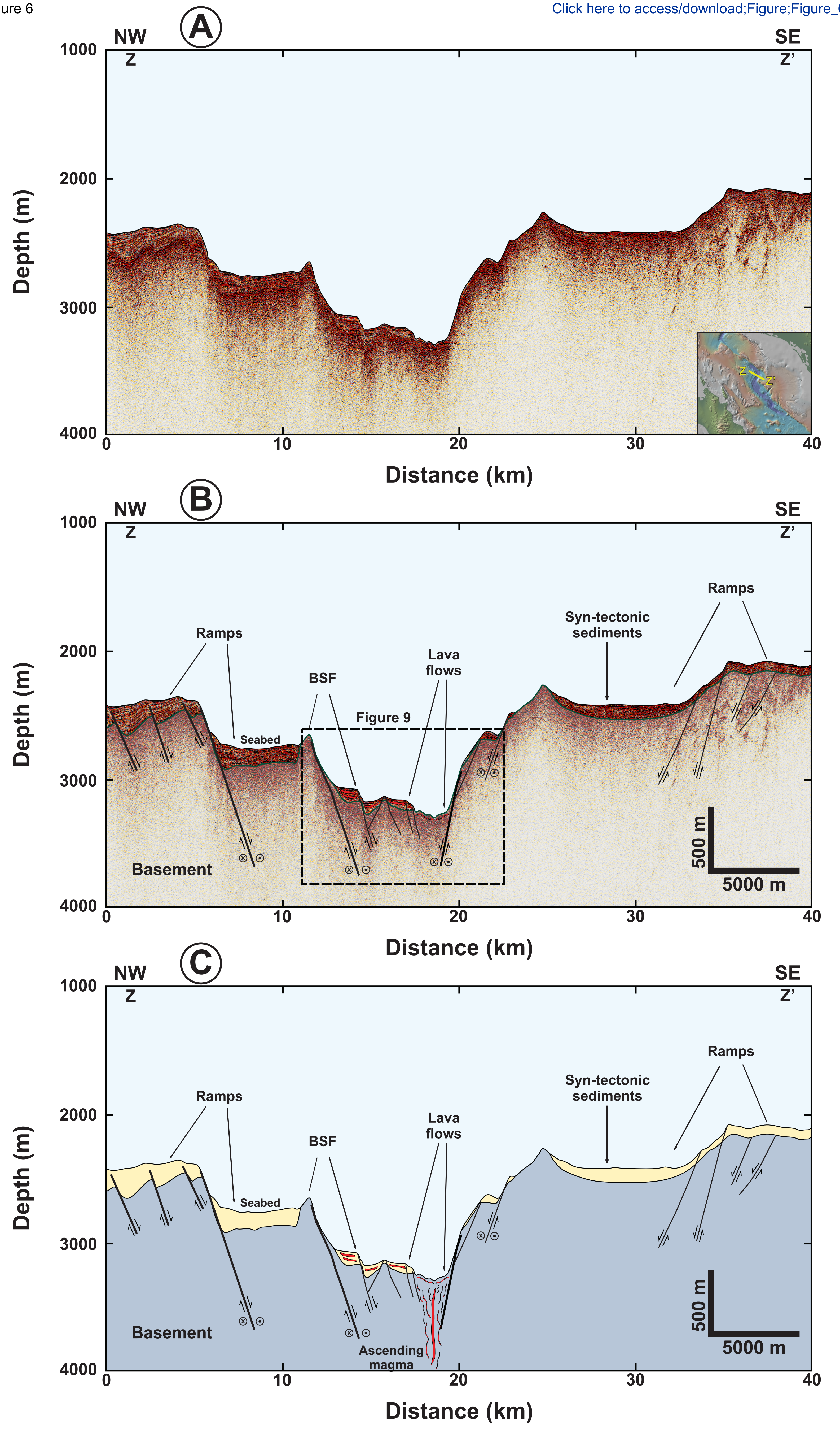

Figure 7

Click here to access/download;Figure;Figure_7.pdf

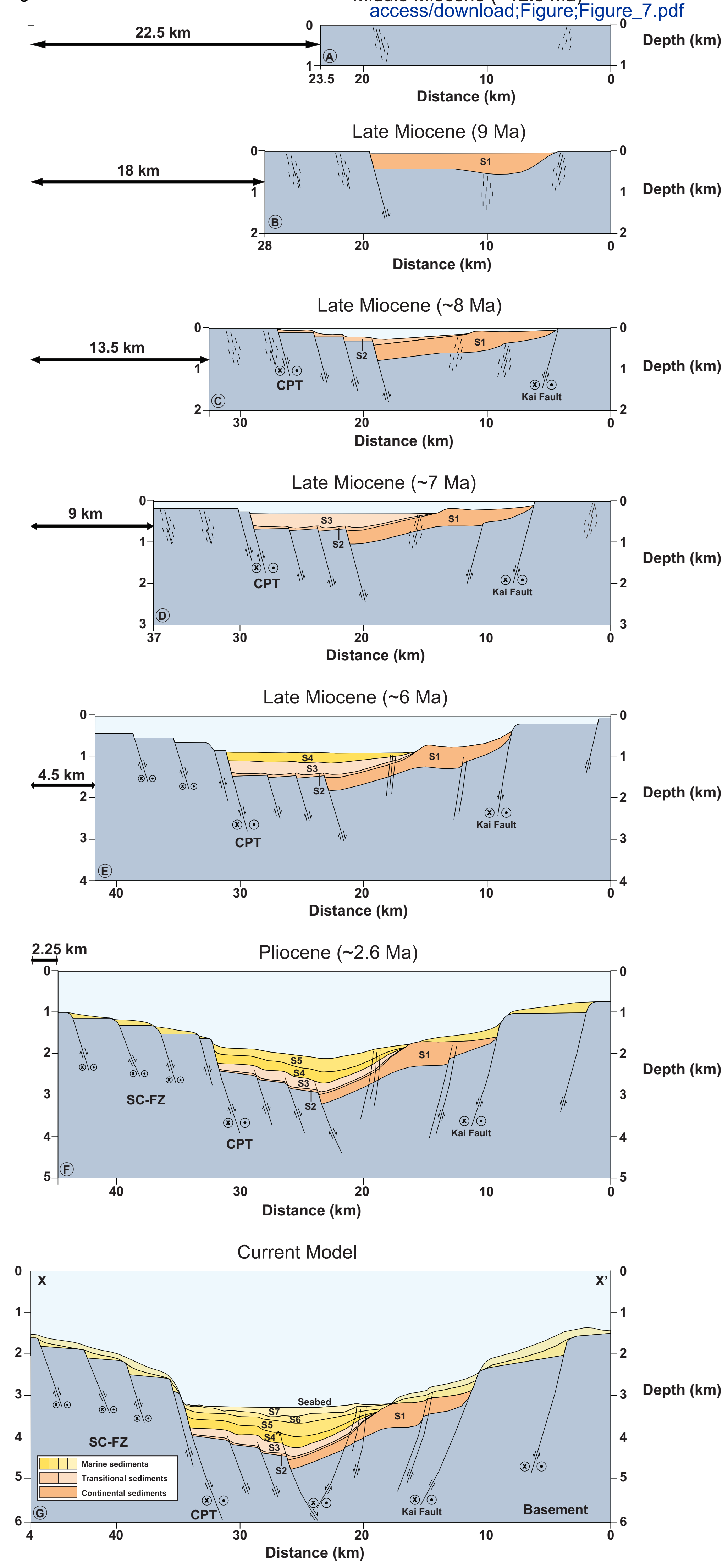

Figure 8

Click here to access/download;Figure;Figure_8.pdf

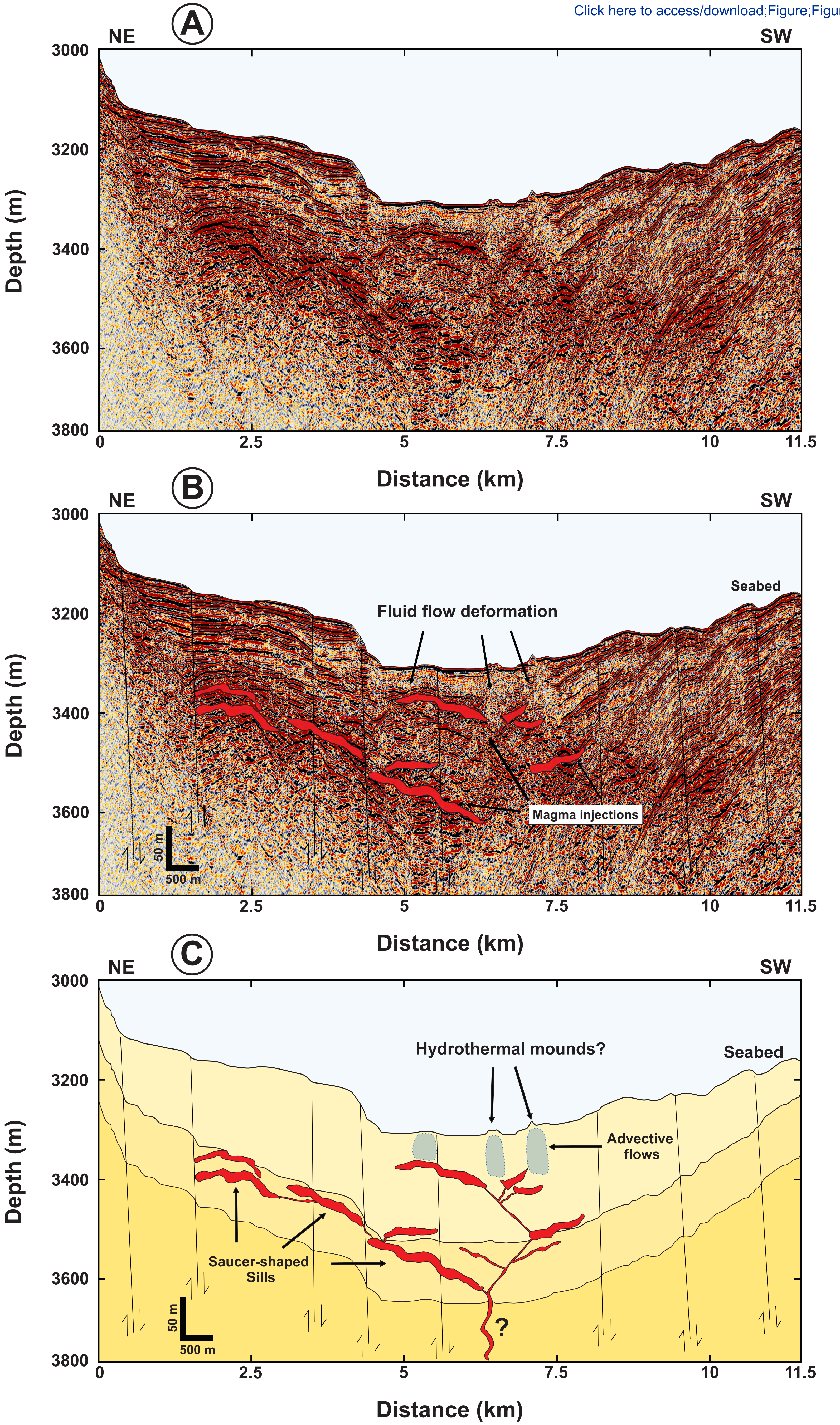

Figure 9

Click here to access/download;Figure;Figure_9.pdf

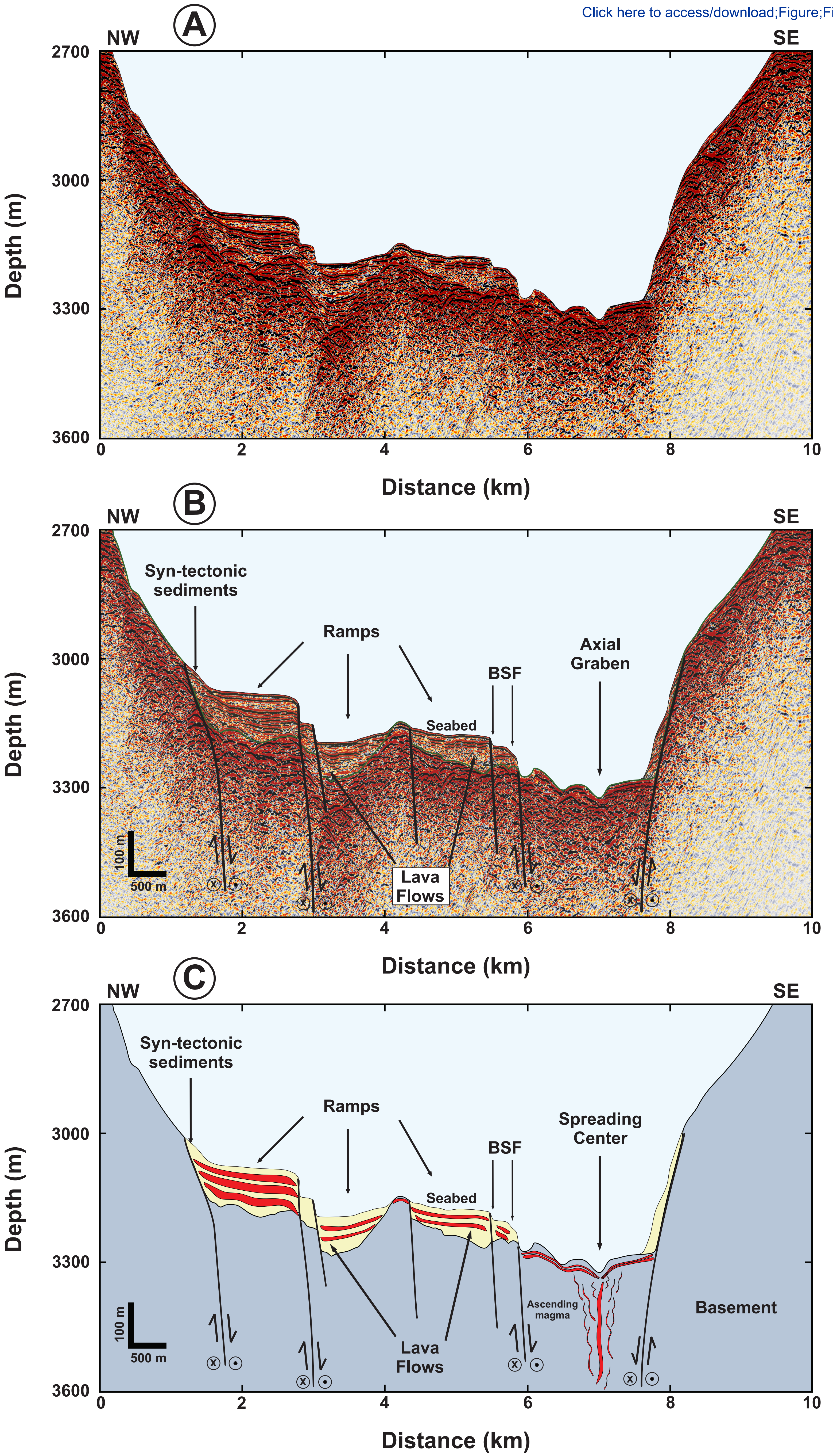

Supporting Information for

Architecture and tectonostratigraphic evolution of the Pescadero Basin Complex, southern Gulf of California: analysis of high-resolution bathymetry data and seismic reflection profiles

Néstor Ramírez-Zerpa[1], Ronald M. Spelz[2]*, Ismael Yarbuh[2], Raquel Negrete-Aranda[3], Juan Contreras[4], David A. Clague[5], Florian Neumann[4], David W. Caress[5], Robert Zierenberg[6], Antonio González-Fernández[7]

[1]*Universidad Autónoma de Baja California. Posgrado en Oceanografía Costera, Facultad de Ciencias Marinas, Ensenada, B.C., México.*

[2]*Universidad Autónoma de Baja California. Departamento de Geología, Facultad de Ciencias Marinas, Ensenada, Baja California, México.*

[3]*Catedrático CONACyT, Laboratorio de Tectonofísica y flujo de calor, Departamento de Geología, Centro de Investigación Científica y de Educación Superior de Ensenada (CICESE). Ensenada, Baja California, México.*

[4]*Laboratorio de Tectonofísica y flujo de calor, Departamento de Geología, Centro de Investigación Científica y de Educación Superior de Ensenada (CICESE), Ensenada, Baja California, México.*

[5]*Monterrey Bay Aquarium Research Institute, Moss Landing, CA. USA.*

[6]*Earth and Planetary Sciences, University of California, Davis, CA, USA.*

[7] *Departamento de Geología, Centro de Investigación Científica y de Educación Superior de Ensenada (CICESE), Ensenada, Baja California, México.*

*corresponding author, rspelz@uabc.edu.mx

Contents of this file

Supporting Information S1

Introduction

This section describes the structural analysis applied to the seismic reflection profile X-X' (Figures 3 and 4 in the main text) in the Pescadero basin Complex (PBC), southern Gulf of California, to quantify fundamental parameters regarding linear strain in 1D. To accomplish this analysis, we measured the horizontal slip of each fault interpreted in the seismic image and employed a series of simple relations using the general principle of area and bed-length preservation (e.g., Chamberlin, 1910). We further contrasted our results with information obtained in the vicinity of the PBC (e.g., Páramo et al., 2008; Brothers et al., 2012; Bot et al., 2016; Macias-Iñiguez et al., 2019) to better constrain the developing stage of the PBC.

Strain analysis of the Pescadero Basin Complex

In classical structural geology, balancing and restoration of cross-sections allows constraint of the kinematic evolution history of a rock body from a pre-deformational state to an actual strained structure. To obtain the initial state (palinspastic section) of the X-X' section in the PBC (Figures 4 and 7 in the main text), we assume rocks as an incompressible deformable material whose kinematics satisfies the continuity equation. We also consider that horizontal compaction, volume loss, and other penetrative deformation mechanisms are negligible. Area-length ratio is conserved, and a balanced cross-section is obtained with good approximation.

The identification and measurement of structural markers were used in the assessment of the magnitude of the crustal extension, e, stretching, s, and strain, ε (Groshong, 1994; Fossen, 2010;

Figure S1; Table S1). These parameters are related through the relations: $e = l_1 - l_0$. Where l_0 is the initial length between markers, and l_1 is their final length, *i.e*., the length measured in the seismic profile (Figure S1). For brittle deformation, the total linear extension, *e*, can be calculated from the sum of the horizontal slip component, e_i, of each one of the faults contained in the seismic image. The change in length and shape (non-rigid deformation) can be expressed in terms of linear strain, *ε,* defined as the ratio in percentage between total deformation and the initial geometry of the extensional system $\varepsilon = \left(\frac{e}{l_0}\right) x\, 100$. Finally, crustal thinning can be expressed in terms of the linear stretching, *s*, a parameter which scales linearly with strain: $s = (\frac{\varepsilon}{100}) + 1$ (Allen and Allen, 2005; Fossen, 2010).

A total of 15 normal faults with dip angles varying between 20 and 80° were interpreted (see Figure 4 in the main text, and Table S1). Our results show that the average slope of the faulting system is 38.2°, which is a typical value of high-angle homogeneous brittle deformation (e.g., Buck, 1993). The magnitude of linear extension, *e*, is ~22.5 km, where fault slip, e_i, varies between ~0.7 and 3.4 km. From the actual length of the seismic reflection profile X-X', we estimate l_1 is in the order of 46 km. Using this value, we calculate the initial state, l_0, of the balanced cross-section is 23.5 km (see Figure 7 in the main text, and Figure S1). Thus, the structural stretch, s, is larger by a factor of 2.0, which results in linear strain of ~96%. According to Fossen (2010), the amount of crustal thinning derived here could be under estimated by a factor of two. This discrepancy can be explained by the low resolution of the seismic reflection profile X-X' at depth where it is difficult to accurately measure finer scale structures (i.e., faults smaller than 50 m in length) (Figure 4).

Thus, we hypothesize that the actual stretching factor in the PBC must be in the order of *s* = 4, similar to the one obtained by other authors in the Alarcon rise and the East Pacific Rise in the mouth of the Gulf of California and the deep waters of the Pacific Ocean, respectively (Páramo et al., 2008, Brothers et al., 2012, Bot et al., 2016; Macias-Iñiguez et al., 2019). The implications of a stretching factor larger than 3 suggest the PBC is controlled by lithospheric thinning associated to decompression melting, resulting in the accretion of new oceanic crust (Foucher et al., 1982; Allen and Allen, 2005).

References

Allen, P.A., & Allen, J.R. (2005). Basin Analysis: Principles And Applications. Second edition: Oxford, UK, Wiley-Blackwell, 549 pp.

Bot, A., Geoffroy, L., Authemayou, C., Bellon, H., Graindorge, D., & Pik, R. (2016). Miocene detachment faulting predating EPR propagation: Southern Baja California: *Tectonics*, 35(5), 1153-1176. https://doi.org/10.1002/2015TC004030

Brothers, D., Harding, A., González-Fernández, A., Holbrook, W.S., Kent, G., Driscoll, N., Fletcher, J.M., Lizarralde, D., Umhoefer, P., & Axen, G. (2012). Farallon slab detachment and deformation of the Magdalena Shelf, southern Baja California: *Geophysical Research Letters*, 39(9), L09307. https://doi.org/10.1029/2011GL050828

Buck, W. R. (1993). Effect of lithospheric thickness on the formation of high-and low-angle normal faults. *Geology*, *21*(10), 933-936. https://doi.org/10.1130/0091-7613(1993)021<0933:EOLTOT>2.3.CO;2

Chamberlin, R. T. (1910). The Appalachian folds of central Pennsylvania. *The Journal of Geology*, *18*(3), 228–251. https://doi.org/10.1086/621722.

Fossen, H. (2010). Structural Geology: Cambridge, U.K, Cambridge University Press, 463 pp.

Foucher, J. P. L., Le Pichon, X., & Sibuet, J. C. (1982). The ocean-continent transition in the uniform lithospheric stretching model: role of partial melting in the mantle. *Philosophical Transactions of the Royal Society of London*. *Series A, Mathematical and Physical Sciences*, *305*(1489), 27-43. https://doi.org/10.1098/rsta.1982.0024

Groshong Jr, R.H. (1994). Area balance, depth to detachment, and strain in extension: *Tectonics*, 13(6), 1488-1497. https://doi.org/10.1029/94TC02020

Macias-Iñiguez, I., Yarbuh, I., Spelz-Madero, R., González-Fernández, A., Fletcher, J. M., Contreras, J., ... & Guardado-France, R. (2019). Modo de extensión de la corteza y formación del Sistema Extensional de Cerralvo, sur del Golfo de California, a partir de datos de reflexión sísmica en 2D. Revista Mexicana de Ciencias Geológicas, 36(3), 334-347. https://doi.org/10.22201/cgeo.20072902e.2019.3.1352

Páramo, P., Holbrook, W.S., Brown, H.E., Lizarralde, D., Fletcher, J., Umhoefer, P., Kent, G., Harding, A., Gonzalez, A., & Axen, G. (2008). Seismic structure of the southern Gulf of California from Los Cabos block to the East Pacific Rise: *Journal of Geophysical Research*, Solid Earth, 113(B3), B03307. https://doi.org/10.1029/2007JB005113

Figure Captions

Figure S1

Simplified reconstruction of the continental crust in the Pescadero Basin Complex (PBC) based on seismic section profile X-X' (see Figures 4 and 7 in the main text). A) The green and red layers have an original length l_0, which corresponds with ~50% of the final state l_1 (see Table S1). For visual purposes, crustal thickness is reduced by a factor of 4 (1:4). B) Final state of the PBC. Zoomed area shows the main structural parameters measured for strain analysis. $\sum e_i$ is the sum of the horizontal slip component of each fault, δ_i is the vertical slip component, and Θ is the dip angle.

Table S1

Summary of one-dimensional strain analysis for seismic profile X-X'.

supplementary data Figure S1

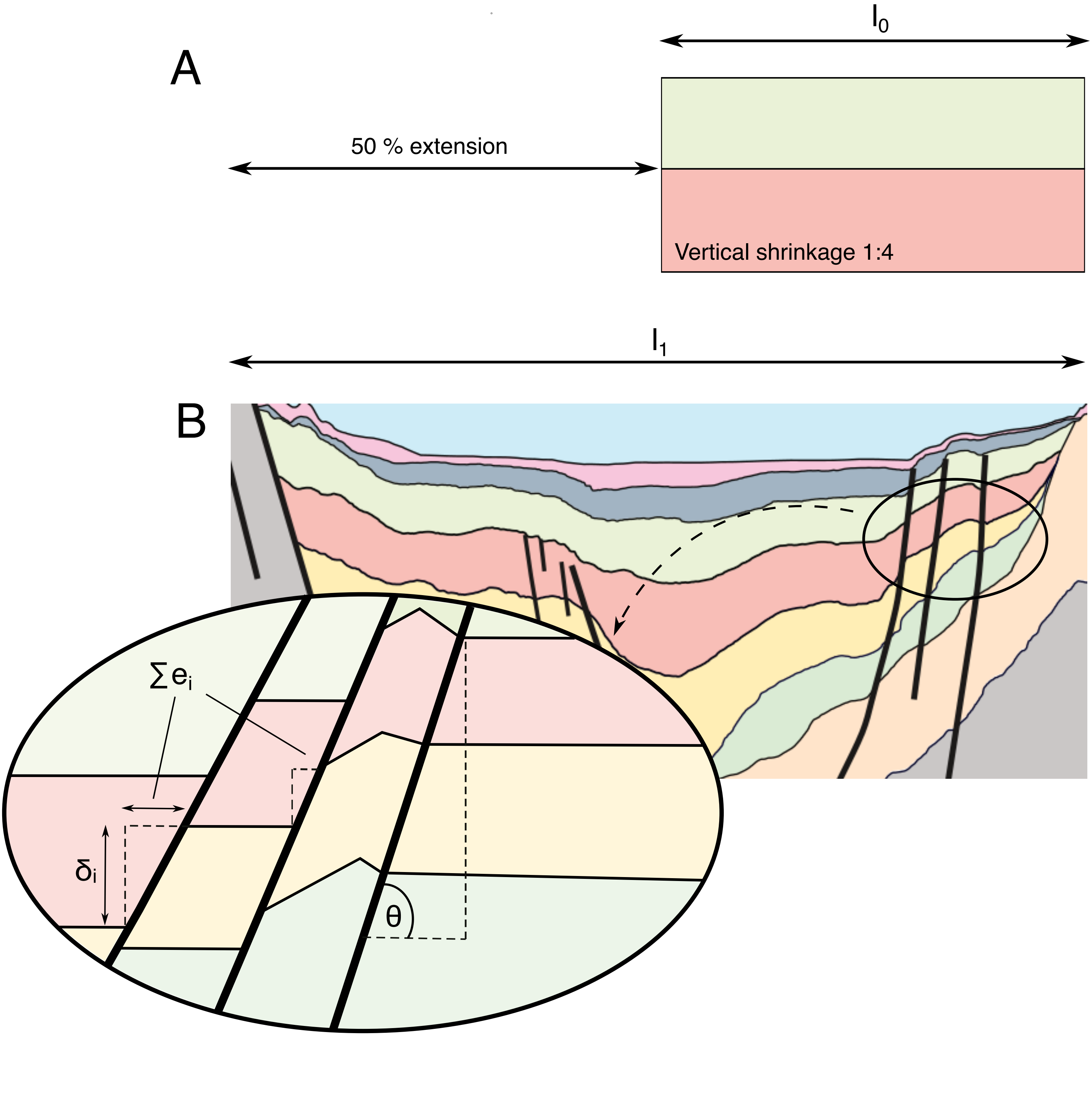

supplementary data Table S1

Table S1. One-dimensional strain analysis for seismic profile X-X'

FAULT	Horizontal deformation (e_i) (m)	Vertical deformation (δ_i) (m)	Dip (Θ) (Degrees)
Santa Cruz Fault Zone (SC fz)	1369	753	32
F-2	1653	595	21
F-3	1574	600	22
F-4	689	463	39
Central Pescadero Transform (CPT)	2595	1389	31
F-6	1132	495	25
F-7	1024	454	25
F-8	3369	1189	20
F-9	2374	1176	28
F-10	532	672	72
F-11	658	929	81
F-12	868	796	53
F-13	855	796	53
Kai fault (Kai f)	1984	1064	31
F-15	1832	1320	41
L_0 = 23492 m	*e* = 22508 m		*Average dip* (Θ) = 38°
L_1 = 46000 m	ε = 96 %	*s* = 2	

Lo= initial length; L_1= final length; *e*= magnitude of extension; ε= linear strain

Θ = fault dip (degrees); *s* = stretching factor.